

# POLITECNICO DI TORINO

Collegio di Ingegneria Chimica e dei Materiali

**Master of Science Course  
in Chemical and Sustainable Processes Engineering**

Master of Science Thesis

## **Starch functionalization: Epoxidation and Methacrylation reactions**



**Tutor**

Prof. Marco Sangermano

.....

**Candidate**

Alessio Truncali

.....

July 2020



*To Salvatore, Liliana,  
Giampiero, Edoardo and Martina.*



## Abstract

Polymeric materials have been widely produced in the world industry in the last decades. These materials present various interesting properties such as high mechanical strength compared to their low density, toughness, corrosion resistance, electrical and thermal insulation and they are also generally low cost. However, synthetic polymers cannot be included in the recycling system causing environmental problems. Functionalized biopolymers constitute a green alternative to the use of polymer derived from fossil fuel resources. The most used sub-class of biopolymers are polysaccharides like starch, cellulose and chitosan. Polysaccharides are biodegradable, low cost and abundant.

In this project two different starch functionalization reactions were conducted: epoxidation and methacrylation. The goal was to obtain functionalized starch derivatives curable under UV light.

Various epoxidation reactions were carried out using epichlorohydrin (ECH) as reagent in a sodium hydroxide (NaOH) solution under nitrogen atmosphere. The NaOH was used as nucleophilic catalyst. Different conditions and stoichiometric ratios were varied and the progress of the reaction was carefully monitored.

Methacrylation reaction was carried out in dimethyl sulfoxide (DMSO) with methacrylic anhydride (MA) as reagent and triethylamine (TEA) as nucleophilic catalyst at room temperature.

Both functionalizations were conducted in stirring conditions and the final products were purified with three precipitation in ethanol.

In order to fully characterize the starting polymer, native maize starch was analysed with different techniques such as Fourier Transform Infrared Spectroscopy (ATR-FTIR), Proton Nuclear Magnetic Resonance ( $^1\text{H-NMR}$ ), Carbon-13 Nuclear Magnetic Resonance ( $^{13}\text{C-NMR}$ ) and Thermogravimetric Analysis (TGA),

The success of both the epoxidized and methacrylated reactions was confirmed by ATR-FTIR,  $^1\text{H-NMR}$  and  $^{13}\text{C-NMR}$  analysis.

The functionalization reactions lead to interesting results which suggest further investigations.

# Table of Contents

<b>1. Introduction</b> .....	<b>1</b>
<b>2. State of Art</b> .....	<b>5</b>
2.1 Polysaccharides.....	5
2.1.1 Polysaccharides Functionalization.....	5
2.2 Starch.....	7
2.2.1 Starch Biosynthesis, Gelatinization Process and Applications.....	8
2.2.2.1 Oxidation.....	11
2.2.2.2 Esterification.....	12
2.2.2.3 Etherification.....	12
2.2.2.4 Epoxidation and Methacrylation.....	14
2.3 Aim of the study.....	16
<b>3. Experimental section</b> .....	<b>18</b>
3.1 Epoxidation reaction.....	18
3.1.1 Materials.....	18
3.1.2 Synthesis.....	18
3.2 Methacrylation Reaction.....	22
3.2.1 Materials.....	22
3.2.2 Synthesis.....	22
<b>4. Methods</b> .....	<b>24</b>
4.1 Nuclear magnetic resonance (NMR).....	24
5.1.1 Proton nuclear magnetic resonance ( <sup>1</sup> H-NMR).....	25
4.1.2 Carbon nuclear magnetic resonance ( <sup>13</sup> C-NMR).....	26
4.2 Attenuated Total Reflectance – Fourier transform infrared (ATR-FTIR) spectroscopy.....	26
4.3 Differential scanning calorimetry (DSC).....	28
4.4 Thermogravimetric analysis (TGA).....	29
<b>5. Results and discussion</b> .....	<b>31</b>
5.1 Maize starch characterization.....	31
5.1.1 ATR-FTIR analysis.....	31
5.1.2 <sup>1</sup> H-NMR analysis.....	32
5.1.3 <sup>13</sup> C-NMR analysis.....	33
5.1.4 DSC analysis.....	33
5.1.5 TGA analysis.....	34
5.2 Epoxidation Reaction.....	35
5.2.1 ES-1, ES-2, ES-3 analysis.....	35
5.2.2 ES-4, ES-5, ES-6 analysis.....	38
5.2.3 ES-9 analysis.....	41

5.2.4 ES-10 analysis.....	43
5.2.5 ES-11 analysis.....	46
5.2.6 ES-12 analysis.....	46
5.3 Methacrylation reaction .....	48
<b>6. Conclusions and future works .....</b>	<b>50</b>
<b>References.....</b>	<b>52</b>
<b>Acknowledgments.....</b>	<b>57</b>



## Sommario

Il seguente lavoro di tesi è incentrato sulla funzionalizzazione dell'amido di mais, mediante le reazioni di epossidazione e metacrilazione, effettuate presso l'università *KTH Royal Institute of Technology* di Stoccolma (Svezia) nel dipartimento di *Fibre and Polymer Technology (FPT)*. Lo scopo principale è dimostrare come la modifica di una sostanza proveniente da materiale organico porti ad interessanti applicazioni. In questo caso l'obiettivo è di ottenere prodotti derivanti dall'amido che possano successivamente essere fotopolimerizzati tramite tecniche con luce UV.

Il primo capitolo è rivolto ad introdurre il tema trattato. Sono stati innanzitutto richiamati i polimeri sintetici descrivendo le proprietà che li rendono particolarmente versatili, ad esempio l'alta resistenza meccanica comparata alla loro bassa densità, la resistenza alla corrosione, l'isolamento termico ed elettrico nonché il basso costo di produzione. D'altro canto, si è fatto riferimento al loro negativo impatto ambientale, dovuto soprattutto all'accumulo di rifiuti plastici a cui consegue un drammatico rilascio di sostanze tossiche.

È stato quindi sottolineato il crescente interesse da parte di attivisti e scienziati sulle possibili alternative ai polimeri derivati dal petrolio. Una delle migliori soluzioni è rappresentata dalla funzionalizzazione di *biopolimeri*, il tema centrale di cui tratterà il seguente lavoro di tesi.

Il termine *biopolimero* indica una tipologia di macromolecole a cui spesso vengono associate tre caratteristiche principali:

*Biodegradabilità*: la capacità di un materiale di essere completamente deteriorato tramite l'attività batterica senza l'emissione di residui tossici, la cui degradazione produce prevalentemente anidride carbonica, metano, acqua e biomassa [3].

*Compostabilità*: la capacità di un materiale organico di essere deteriorato mediante processo di compostaggio. Un trattamento che, mediante azione aerobica produce il compost, una sostanza fangosa utilizzabile per l'agricoltura [4].

*Bio-based*: termine applicato ai polimeri derivanti da fonti rinnovabili.

Nel corso del secondo capitolo di questo elaborato si è fatto riferimento allo stato dell'arte. Dopo un breve cenno alle caratteristiche chimiche dei polisaccaridi, sono presentate schematicamente le loro principali tecniche di modifica (chimiche, fisiche e biologiche) [7]. I polisaccaridi sono sostanze facilmente reperibili ed economiche e presentano delle proprietà chimico-fisiche di base che li rendono potenzialmente interessanti per una vasta gamma di applicazioni. La funzionalizzazione, intesa come modifica tramite l'introduzione di determinati gruppi funzionali all'interno della struttura molecolare, permette di migliorarne le caratteristiche, trasformandoli spesso in prodotti competitivi anche in termini di costi, se confrontati con i polimeri sintetici. Tuttavia, le modifiche effettuate sui polisaccaridi sono tutt'altro che prive di insidie. Le loro proprietà biologiche li rendono, durante gli esperimenti, facili alla disgregazione, suscettibili agli attacchi batterici e all'interazione con enzimi estranei. Inoltre, si ha spesso, durante le prove sperimentali, la presenza di reazioni collaterali che portano alla formazione di prodotti indesiderati, fenomeno che va sotto il nome di *regioselettività* [10].

Nella seconda parte di questo capitolo viene focalizzata l'attenzione sulla sostanza oggetto di studio: l'amido, polisaccaride le cui potenziali applicazioni sono ancora in fase di approfondimento. La sua composizione chimica è caratterizzata dalla ripetizione di numerosi anelli esagonali di glucosio ( $C_6H_{10}O_5$ ) ed è strutturalmente formato da due tipi di conformazione macromolecolari: amilosio (lineare) ed amilopectina (ramificata) mostrate in Figura 1.

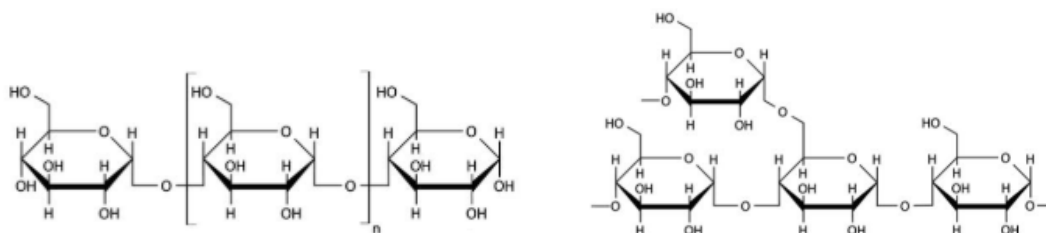


**Figura 1:** struttura chimica dell'amido: amilosio (a) e amilopectina (b).

L'obiettivo sperimentale di questo lavoro è quello di sostituire i gruppi ossidrilici dell'unità glicosidica dell'amido con gruppi epossidici, tramite reazione di epossidazione, o metacrilici, tramite reazione di metacrilazione.

In seguito, è stata descritta la procedura di biosintesi dell'amido a partire dai cloroplasti [16] ed il fenomeno di gelatinizzazione a cui è soggetto in acqua a seguito di un aumento di temperatura [15]. Infine, sono stati approfonditi esempi di tecniche di funzionalizzazione dell'amido, sottolineandone le interessanti applicazioni, terminando la trattazione sullo stato dell'arte con focus sulle funzionalizzazioni di epossidazione e sulla metacrilazione presenti in letteratura, fornendo interessanti spunti di partenza per l'esecuzione dei successivi esperimenti.

Il terzo capitolo di questo elaborato descrive i procedimenti ed i materiali utilizzati nel lavoro sperimentale. Vengono quindi illustrati i protocolli di reazione di epossidazione e metacrilazione eseguiti in questo lavoro.

I reagenti utilizzati per la reazione di epossidazione sono gli *epossidi*: anelli chiusi a forma triangolare costituiti da tre elementi. La struttura di base è costituita da due atomi di carbonio legati ad un atomo di ossigeno. La loro forte tensione di legame li rende altamente reattivi, se comparati ad altri eteri. In questo caso si è utilizzato come reagente l'epicloridrina (ECH), un composto incolore, volatile, tossico, infiammabile che emana un odore pungente. Come catalizzatore nucleofilo per la reazione è stato utilizzato idrossido di sodio (NaOH).

Nel corso delle prime prove sono stati posti innanzitutto 100 ml di acqua deionizzata in un'ampolla a tre uscite ed è stato aggiunto approssimativamente 1 g. di amido in condizioni miscelate. La soluzione è stata gradualmente riscaldata e mantenuta per mezz'ora a quella temperatura portando l'amido a gelatinizzazione. In seguito, l'ampolla è stata equipaggiata di un condensatore ed un iniettore di azoto per ventilare l'ambiente di reazione. Quindi l'ECH è stata aggiunta a gocce con una siringa. Il prodotto è stato infine precipitato e lavato tre volte con eccesso di etanolo (EtOH).

Il set-up ed il prodotto finale della reazione sono presentati nelle seguente Figura 2.

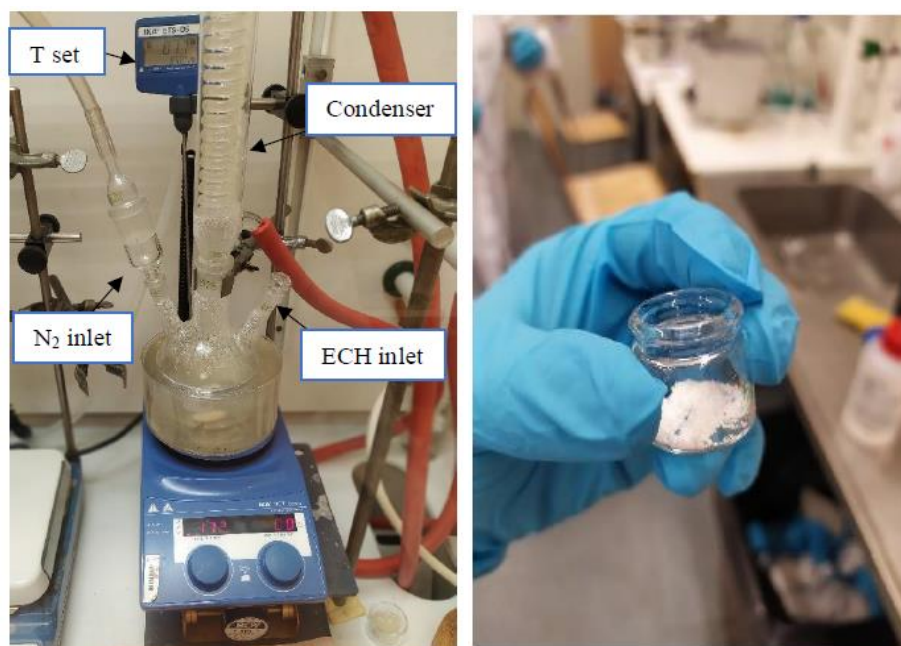


**Figura 2:** set-up (a) e prodotto finale (b) della reazione di epossidazione.

Nel corso dei primi esperimenti, il pH è stato costantemente monitorato e tenuto ad un valore all'incirca pari ad 8, aggiungendo determinate quantità di soluzione 0.5 M di NaOH con il procedere della reazione. Dal sesto batch in poi, un esatto quantitativo di soluzione basica è stata invece introdotta dall'inizio. Nella seguente Tabella 1 sono schematizzati i primi otto esperimenti condotti.

**Tabella 1:** Riassunto delle condizioni di reazione di epossidazione (dalla 1 alla 8)

Reazione	Amido [g]	ECH [ml]	Rapporti molari (ECH: <sup>1</sup> AGU:NaOH)	Soluzione 0.5 M NaOH [ml]	Tempo [h]	Temperatura [°C]
ES-1	1.00	0.48	1:1: -	undefined	2	85
ES-2	1.03	1.00	2:1: -	undefined	2	85
ES-3	1.01	1.47	3:1: -	undefined	2	85
ES-4	1.03	2.49	5:1: -	undefined	2	85
ES-5	1.07	0.52	1:1: -	undefined	2	100
ES-6	1.04	3.52	7:1:1	12.83	5	85
ES-7	1.10	3.74	7:1:1	13.62	5	85
ES-8	1.10	6.39	12:1:1	13.58	5	85

<sup>1</sup>AGU: unità glicosidica

Dalla reazione 9 alla 12 (Tabella 2), la differenza maggiore è stata l'introduzione di un certo quantitativo della soluzione 0.5 M di NaOH dall'inizio degli esperimenti, senza l'aggiunta di ulteriore acqua deionizzata.

**Tabella 2:** Riassunto delle condizioni di reazione di epossidazione (dalla 1 alla 8)

Reaction	Starch [g]	ECH [ml]	Molar ratio (ECH:AGU:NaOH)	NaOH Solution [ml]	Time [h]	Temperature [°C]
ES-9	1.16	6.70	12:1:12	171.85	5	85
ES-10	1.06	7,79	15:1:15	196	5	85
ES-11	1.05	8,64	17:1:17	220	5	85
ES-12	1.02	9,87	20:1:20	251,8	5	85

La seguente Figura 3 mostra la schematizzazione della reazione epossidazione ed una delle possibili strutture dell'amido epossidato.

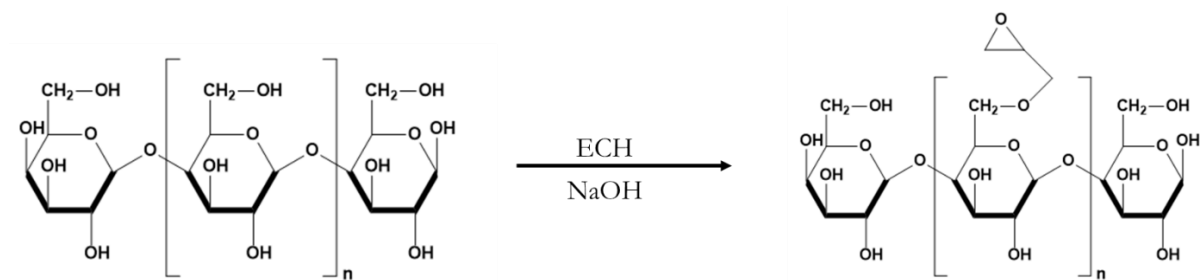


**Figura 3:** illustrazione schematica della reazione di epossidazione dell'amido. La struttura finale presentata è solo una tra le tante possibili e presuppone la sostituzione di un solo gruppo ossidrilico

Sotto è presentato il protocollo per la reazione di Metacrilazione.

Inizialmente 6 [g.] di amido di mais sono stato posti in un'ampolla ad una uscita insieme a dimetilsolfossido (DMSO), utilizzato come reagente. La temperatura è stata incrementata a 70 [°C]. Dopo 30 minuti l'amido è stato gelatinizzato e la soluzione è stata raffreddata a temperatura ambiente. L'andride metacrilica è stata quindi aggiunta a gocce con una siringa e la trietilammina (TEA), utilizzata come catalizzatore nucleofilo, è stata introdotta lentamente (rapporto molare AGU:MA:TEA du 1:2:0.04). La soluzione finale è stata mantenuta a temperatura ambiente per 18 ore.

Dopo questo lasso di tempo, il prodotto è stato precipitato in etanolo, dissolto in acqua deionizzata e di nuovo in etanolo. Questa procedura è stata ripetuta due volte per purificare il prodotto. La soluzione finale è stata quindi liofilizzata.

Il set-up della reazione ed il prodotto finale sono mostrati nella seguente Figura 4.



**Figura 4:** set-up (a) e prodotto finale (b) della reazione di metacrilazione.

La reazione di metacrilazione con una delle possibili strutture dell'amido metacrilato è mostrata in Figura 5.

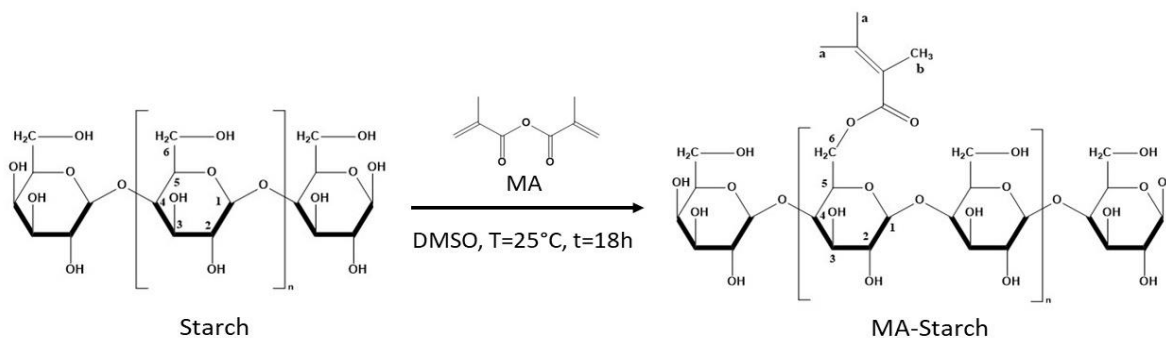


**Figura 5:** illustrazione schematica della reazione di metacrilazione dell'amido. La struttura finale presentata è solo una tra le tante possibili e presuppone la sostituzione di un solo gruppo ossidrilico

Il quarto capitolo di questo studio descrive le tecniche di caratterizzazione che sono state utilizzate per:

- Caratterizzare l'amido di partenza
- Caratterizzare i prodotti delle reazioni di epossidazione e metacrilazione

La spettroscopia infrarossa in riflettanza totale attenuata (ATR-FTIR) è stata eseguita utilizzando lo spettrometro Perkin-Elmer Spectrum 2000 (16 scansioni, risoluzione  $4\text{ cm}^{-1}$ ) con l'intenzione di verificare la presenza di gruppi epossidici e metacrilici del polimero funzionalizzato. Prima di testare ogni campione è stato eseguito un background in cui gli spettri sono stati registrati eseguendo 16 scansioni in un range di lunghezze d'onda compreso tra  $4000$  e  $650\text{ cm}^{-1}$ .

La risonanza magnetica protonica ( $^1\text{H-NMR}$ ) e carbonica, entrambe con strumento Avance 400 (400.13 MHz-Bruker USA), sono state eseguite a temperatura ambiente, ponendo 8 mg. di campione in 1 ml di DMSO- $d_6$  (deuterato). Tramite software MestReNova si sono potuti individuare i  $\delta$ -shift dei vari spettri analizzati, permettendo di verificare l'efficacia della funzionalizzazione, grazie alla variazione dell'intorno chimico degli atomi di idrogeno e di carbonio delle unità terminali.

La calorimetria differenziale a scansione (DSC) ha consentito di valutare le variazioni della temperatura di transizione vetrosa ( $T_g$ ) prima e dopo la funzionalizzazione. Le misurazioni sono state eseguite su campioni di circa 7 mg. usando un Mettler Toldedo DSC 820. Il flusso di calore applicato è stato di 10  $^{\circ}\text{C}/\text{min}$  sotto flusso di azoto (50  $\mu\text{l}/\text{min}$ ).

L'analisi termogravimetrica (TGA) è stata utilizzata per valutare la stabilità termica sia dell'amido di partenza che dei prodotti funzionalizzati. Le misure sono state eseguite con test tra 15  $^{\circ}\text{C}$  e 800 $^{\circ}\text{C}$  sotto flusso di azoto, usando un TGA Mettler Toledo. I risultati sono stati analizzati usando il software STARE.

Nel quinto capitolo sono riportati e discussi i risultati delle prove di caratterizzazione. Esso è strutturato in tre sezioni:

1. Caratterizzazione dell'amido di partenza
2. Caratterizzazione dei prodotti derivati dall'eossidazione
3. Caratterizzazione dei prodotti derivati dalla metacrilazione

Gli spettri ATR-FTIR,  $^1\text{H-NMR}$  e  $^{13}\text{C-NMR}$  dell'amido di partenza si sono rilevati coerenti con la struttura della molecola. La calorimetria a scansione differenziale (DSC) ha fornito una temperatura di transizione vetrosa ( $T_g$ ) pari a 107  $^{\circ}\text{C}$  con una deviazione standard di 2.9  $^{\circ}\text{C}$ . La temperatura di degradazione trovata con l'analisi termogravimetrica (TGA) è di 309.9  $^{\circ}\text{C}$ .

Sono stati quindi analizzati i prodotti delle reazioni di eossidazione. Negli spettri FTIR delle reazioni quattro e cinque presentate nella seguente Figura 6, non sono state notate significative differenze rispetto all'amido di riferimento. Nella sesta reazione lo spettro presenta invece due nuovi picchi a 1260  $\text{cm}^{-1}$  e 796  $\text{cm}^{-1}$ . Il primo può essere attribuito alle vibrazioni di stretching del legame etere C-O-C, possibilmente dovuto ad un certo quantitativo di anelli epossidici aperti [37]. L'altro picco può essere attribuito all'anello epossidico monosostituito [34]. Tuttavia, i segnali di questi due nuovi picchi hanno una bassa assorbanza. Ciò indica che i risultati ottenuti hanno un alto grado di incertezza.

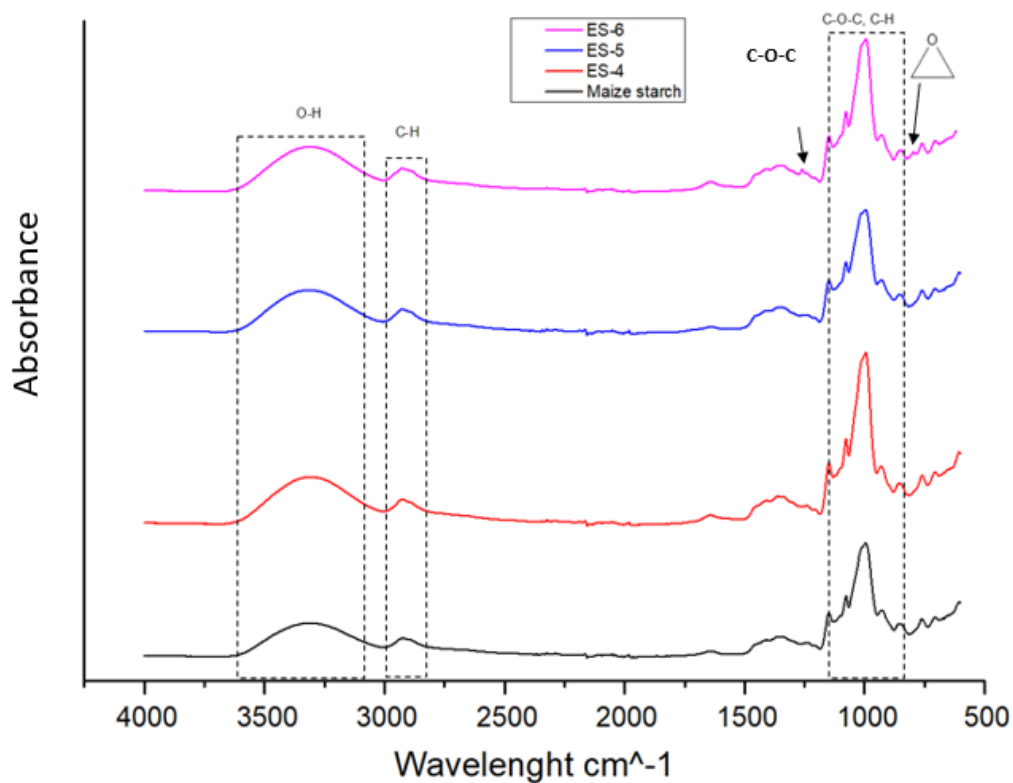


**Figura 6:** spettri FTIR di amido di mais e dei prodotti di reazione ES-4, ES-5, ES-6.

La Figura 7 seguente mostra lo spettro  $^1\text{H-NMR}$  delle reazioni precedenti. Il campione della sesta reazione era poco solubile in  $\text{DMSO-d}_6$  pertanto i picchi dello spettro sono risultati poco marcati e quindi difficile da analizzare. Tale problematica è stata riscontrata anche nelle prove successive.

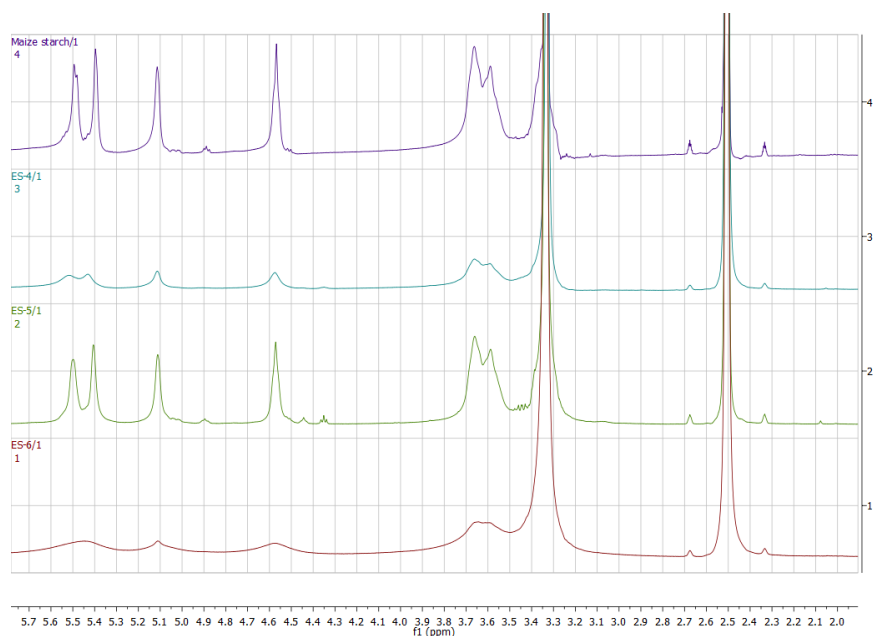


**Figura 7:** spettri  $^1\text{H-NMR}$  di amido di mais e dei prodotti di reazione ES-4, ES-5, ES-6.

Dalla reazione nove, la scelta di aggiungere un determinato quantitativo di soluzione di NaOH dall'inizio dell'esperimento e senza l'introduzione di ulteriore acqua deionizzata ha portato a risultati più evidenti. In particolar modo l'analisi FTIR della reazione numero 10 (ES-10), mostrata in Figura 8, ha rilevato la presenza di nuovi picchi. Le curve per questo esperimento sono state riportate estrapolando dei campioni a diversi intervalli di tempo di reazione fino ad un massimo di 5 ore. Si osserva un decremento della regione attribuita alla vibrazione dei legami -OH, nel range tra  $3650-3000\text{ cm}^{-1}$  [39] [40] [41] [42] denotando un abbassamento dei quantitativi di gruppi ossidrilici. Il nuovo picco a  $1550\text{ cm}^{-1}$  ed il graduale incremento dell'intensità del picco a  $1431\text{ cm}^{-1}$  sono attribuiti alla vibrazione dovuta alla flessione del legame  $-\text{CH}_2-$  [34] [39] [40] [45] [46] che potrebbe indicare la presenza di gruppi etere. Il picco a  $879\text{ cm}^{-1}$ , la cui intensità aumenta con il procedere della reazione, può essere assegnata alla vibrazione dovuta allo stretching del legame C-O-C dell'anello epossidico come confermato in letteratura [39][40] [41] [42] [44] [45] [46] [47]. Tuttavia, quest'ultimo segnale è parzialmente sovrapposto dalla vibrazione di stretching e flessione del legame C-OH e dalla vibrazione del legame tra le unità glicosidiche C-O-C (carbonio -  $\alpha$ ) [34] [40].

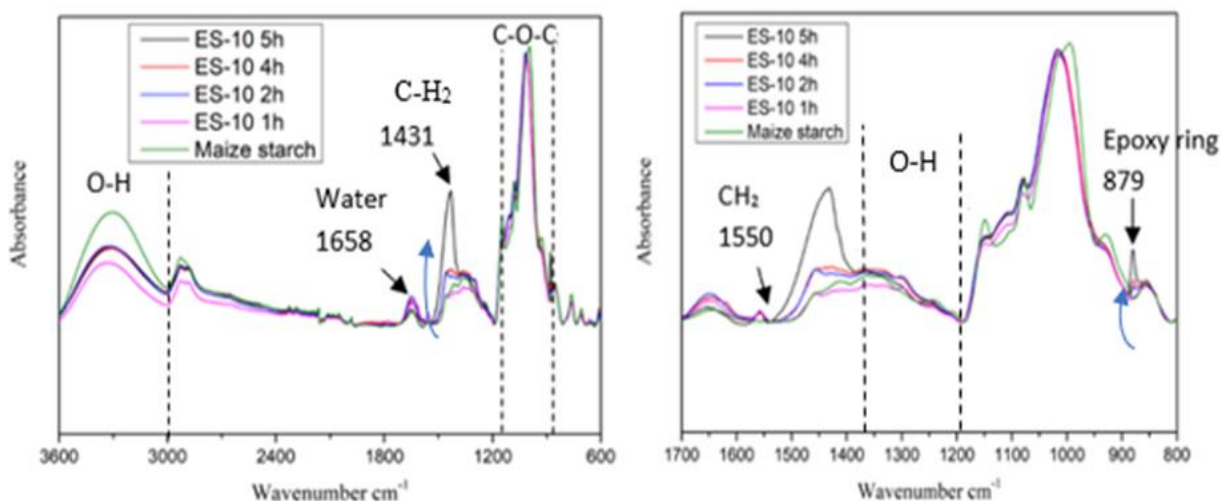


**Figura 8:** spettri FTIR di amido di mais e dei prodotti di ES-10 a diversi tempi di reazione

L'analisi  $^1\text{H-NMR}$  non ha purtroppo fornito risultati esaustivi per i problemi di solubilità affermati in precedenza e non è stata dunque riportata.

L'analisi TGA in Figura 9 mostra le differenze sulla stabilità termica tra l'amido di riferimento ed un campione del prodotto della reazione 10 dopo 5 ore. La degradazione dell'amido modificato inizia a circa  $220\text{ }^\circ\text{C}$  mentre la temperatura in corrispondenza della massima perdita di peso, rappresentata dal flesso della curva  $T_0 = \text{dm}/\text{dT}_{\text{max}}$ , si ha a circa  $261\text{ }^\circ\text{C}$ . Per l'amido non modificato la degradazione inizia a  $250\text{ }^\circ\text{C}$ , mentre la perdita massima di peso si ha a circa  $310\text{ }^\circ\text{C}$ . Tuttavia, nonostante la degradazione dell'amido modificato avvenga a temperature più basse, le percentuali in peso residue alla medesima temperatura risultano maggiori rispetto a quelle dell'amido non modificato. Questo indica che probabilmente il prodotto di reazione risulta essere più resistente ai trattamenti termici rispetto alla sostanza di partenza.

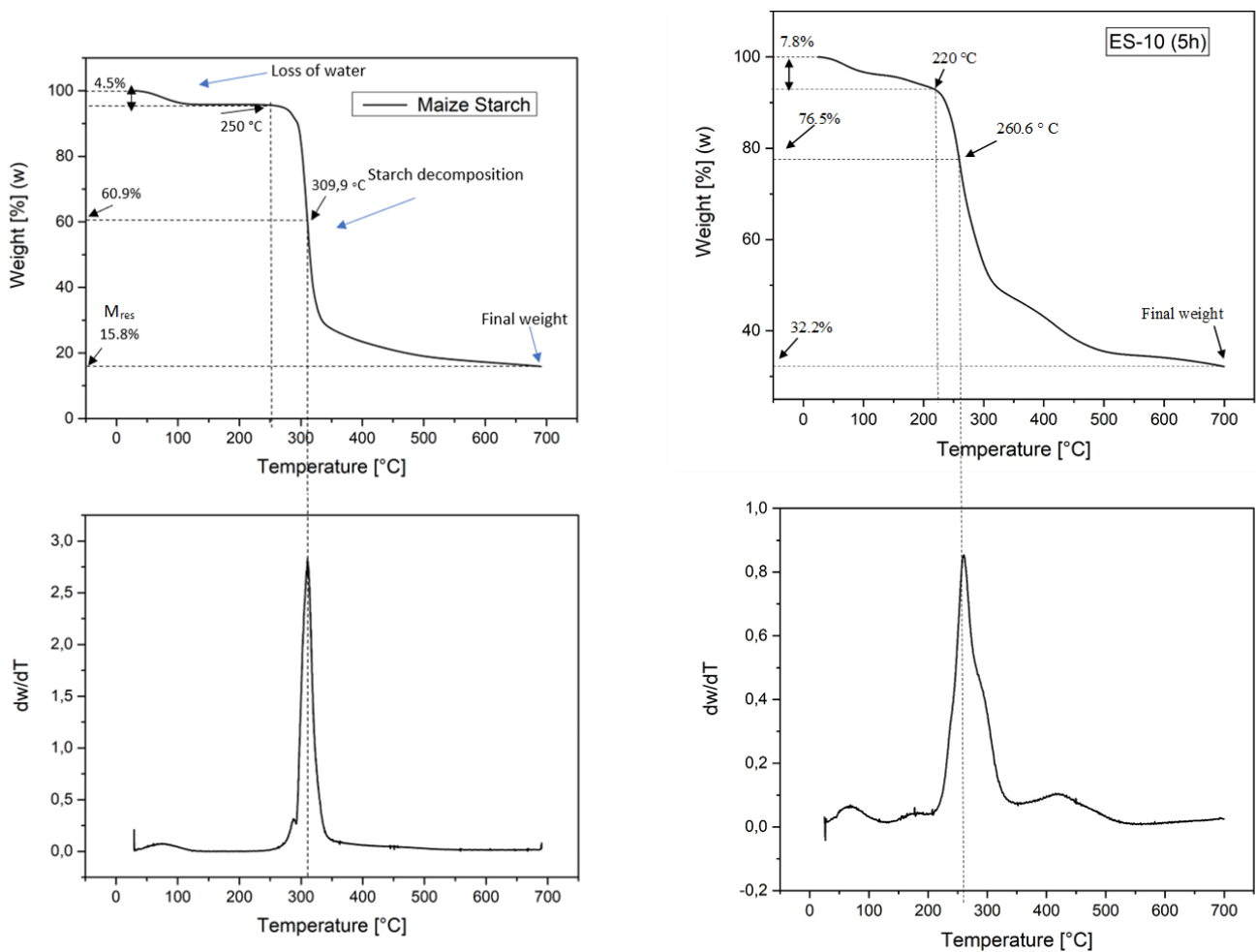


**Figura 9:** confronto TGA tra amido di mais e prodotto di reazione ES-10 dopo 5 ore.

Tuttavia, i problemi di regioselettività della funzionalizzazione dei biopolimeri che sono stati introdotti nel capitolo introduttivo, potrebbero portare a reazioni competitive. Alcuni dei prodotti ipotizzati sono illustrati nella seguente Figura 10.

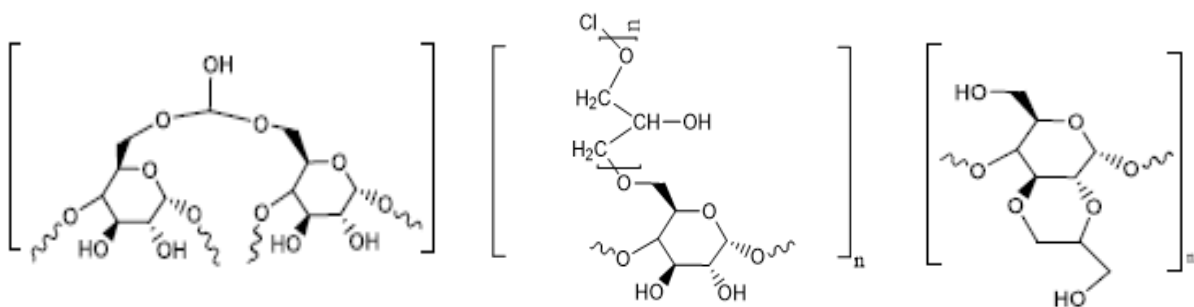


**Figura 10:** prodotti di reazione competitive ipotizzati per ES-10.

Infine, sono stati analizzati i prodotti della reazione di metacrilazione. La comparazione tra gli spettri  $^1\text{H-NMR}$  dell'amido metacrilato e dell'amido grezzo mostrati in Figura 11, conferma la presenza di caratteristici picchi assegnati al doppio legame metacrilico  $=\text{CH}_2$  (5.66 e 6.07 ppm) ed ai gruppi metilici  $-\text{CH}_3$  (1.9 ppm). Il grado di sostituzione (DS) è stato calcolato come il rapporto degli integrali dei picchi  $^1\text{H-NMR}$  usando la seguente equazione (1) [50].

$$DS = \left(\frac{I_{1.9}}{3}\right) / I_{5.11} \quad (1)$$

Dove:

- $I_{1.9}$  è l'integrale dell'intensità del  $\text{CH}_3$  (denominato *b* negli spettri)
- $I_{5.11}$  è l'integrale di intensità del protone dell'unità glicosidica in posizione 1H (carbonio- $\alpha$ )

La divisione per 3 è dovuta alla presenza dei tre gruppi  $-\text{OH}$  in ogni unità glicosidica. Il DS ottenuto è stato 0.08 dato che  $I_{1.9} = 0.75$  e  $I_{5.11} = 1$ . Questo vuol dire che c'è solo un gruppo alcolico metacrilato ogni quattro unità glicosidiche come mostrato in figura 9 [50].

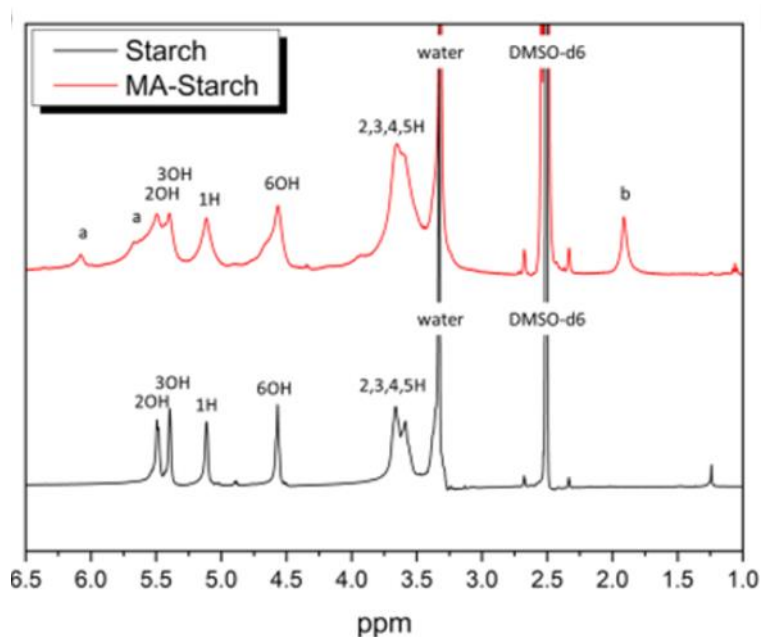


**Figura 11:** spettri  $^1\text{H-NMR}$  per l'amido di mais e l'amido metacrilato [50].

Nella Figura 12 seguente sono mostrati gli spettri  $^{13}\text{C-NMR}$  dell'amido metacrilato e dell'amido di riferimento. Sono visibili i segnali del gruppo metacrilato a 18.45 ppm (carbonio metilico), 136.61 e 127.75 ppm (carbonio a doppio legame) e il 170.38 ppm attribuito al carbonio  $\text{C}=\text{O}$  [50].

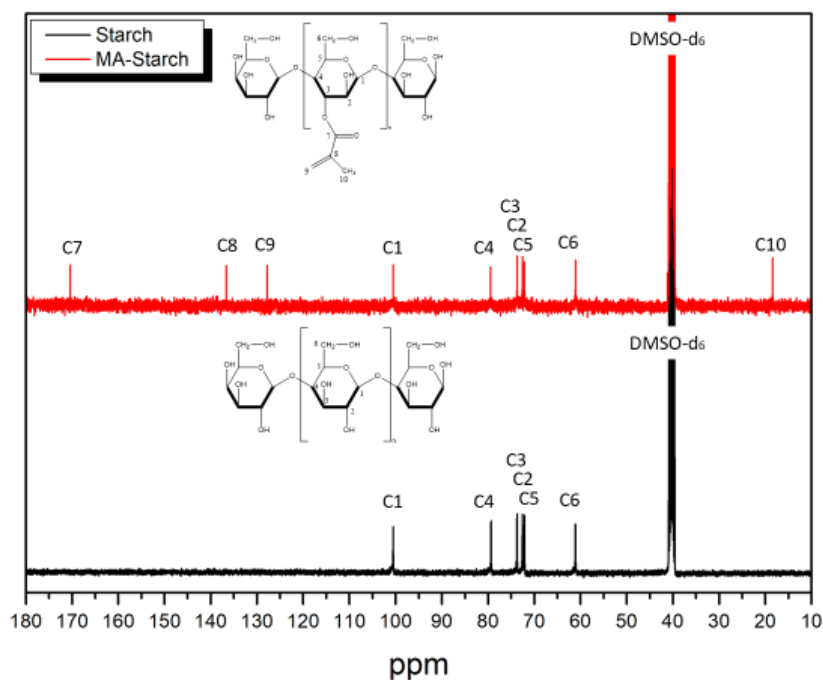


**Figura 12:** spettri  $^{13}\text{C}$ -NMR per l'amido di mais e metacrilato [50].

La Figura 13 seguente riporta una comparazione tra gli spettri FTIR dell'amido grezzo e dell'amido metacrilato. Nello spettro FTIR dell'amido modificato sono visibili due nuovi picchi acuti a  $1709$  e  $1640\text{ cm}^{-1}$  che possono rispettivamente essere attribuiti alla vibrazione di stretching del legame presenti nel gruppo estero  $\text{C}=\text{O}$  e  $-\text{CO}-$ . Questi risultati suggeriscono un riuscito innesto dei gruppi metacrilati nella struttura dell'amido [50].

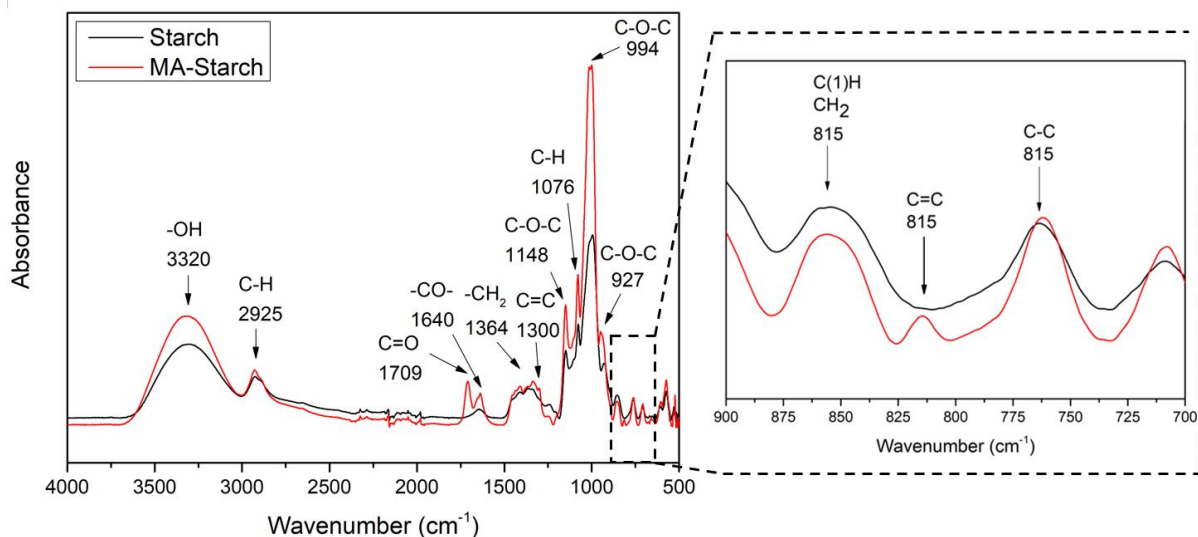


**Figura 13:** spettri FTIR di amidi di mais e metacrilato [50].

Per concludere, le reazioni di epossidazione hanno prodotto dei risultati interessanti soprattutto a partire dalla 9, quando è stato utilizzato un determinato quantitativo di soluzione 0.5 M di NaOH dall'inizio degli esperimenti, senza l'introduzione di ulteriore acqua distillata. La presenza degli anelli epossidici è stata confermata attraverso le analisi FTIR, in particolare monitorando i prodotti della reazione 10 a diversi intervalli di tempo.

La reazione di metacrilazione ha prodotto risultati significativi. La presenza del doppio legame metacrilico  $=CH_2$  e dei gruppi metilici  $-CH_3$  è stata confermata attraverso le analisi spettroscopiche ed il calcolo del grado di sostituzione.

I problemi principali nel corso di questo progetto sono stati relativi alle analisi  $^1H$ -NMR in quanto i prodotti di epossidazione erano poco solubili in DMSO- $d_6$ , rendendo difficoltosa se non impossibile la lettura degli spettri.

Ulteriori analisi potranno successivamente dare conferma della buona riuscita delle funzionalizzazioni eseguite. Pertanto, vengono proposti i seguenti punti, che non sono stati condotti per mancanza di tempo e per il particolare periodo storico in cui questo lavoro si è inserito:

1. Condurre le analisi  $^1H$ -NMR ad alta temperatura per i prodotti di epossidazione, al fine di solubilizzarli in DMSO- $d_6$ ;
2. Eseguire procedure di titolazione per calcolare il grado di sostituzione degli anelli epossidici. Tuttavia, non è semplice trovare una soluzione capace di dissolvere adeguatamente i prodotti di reazione;
3. Testare le effettive applicazioni dei prodotti finali, performando la fotopolimerizzazione tramite tecniche con luce UV.





## 1. Introduction

Polymeric materials derived from petroleum are widely used in the world of industry. These materials present various interesting properties such as high mechanical strength compared to their low density, toughness, corrosion resistance, electrical and thermal insulation and they are generally low-cost [1]. However, the growing of synthetic polymers creates several environmental and human health problems. In fact, most of them are not biodegradable and if they are disposed in the landfills slowly leak toxins into the soil. For these reasons, all around the world green movements and activists are pressing the highest levels of government to reduce the amount of plastic waste.

In order to solve these problems, a great number of scientists have focused their attention to find alternatives to the petroleum-based polymers. One of the best solutions is represented by the functionalization of biological macromolecules, called biopolymers. The word “Biopolymer” is often associated with three main adjectives: biodegradable, compostable and bio-derived [2]. However, it does not mean that a biopolymer possesses all these qualities at the same time. Below the meaning of each adjectives will be analysed.

- *Biodegradable*: means that the material fully deteriorates in ambient condition through the microbial activity of aerobic or anaerobic bacteria without leaving any toxic residue. The bio-polymers degradation produces carbon dioxide, methane, water, inorganic compounds, or biomass (Figure 1.1) [3].

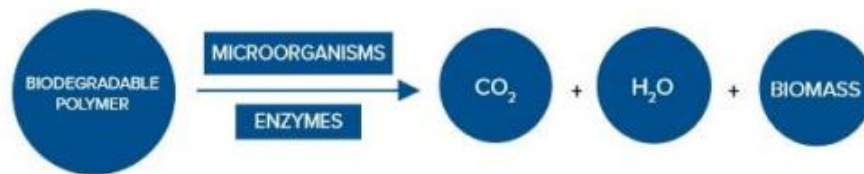


**Figure 1.1:** polymers biodegradation process [3].

- *Compostable*: an organic material is compostable when it needs to be treated with the composting process to be fully degraded. Composting is an aerobic biodegradation process which leads to the production of compost. The term compost refers to a material with the same characteristics of the dark loam used for cultivation. Generally, the composting process is faster than the biodegradation one but can only happen at fixed condition. [4].
- *Bio-based*: is a term applied to polymers arising from renewable sources. The determination of the bio-based content into a polymer can be calculate from the amount of bio-based carbon as a fraction of the total organic carbon content.

In Figure 1.2 is reported the annual global plastic production measured in tonnes per year, from 1950 to 2018. The short downturn in annual production in 2009 and 2010 was the result of the 2008 global financial crisis. The graph underlines how biopolymers production is increasing in recent years.

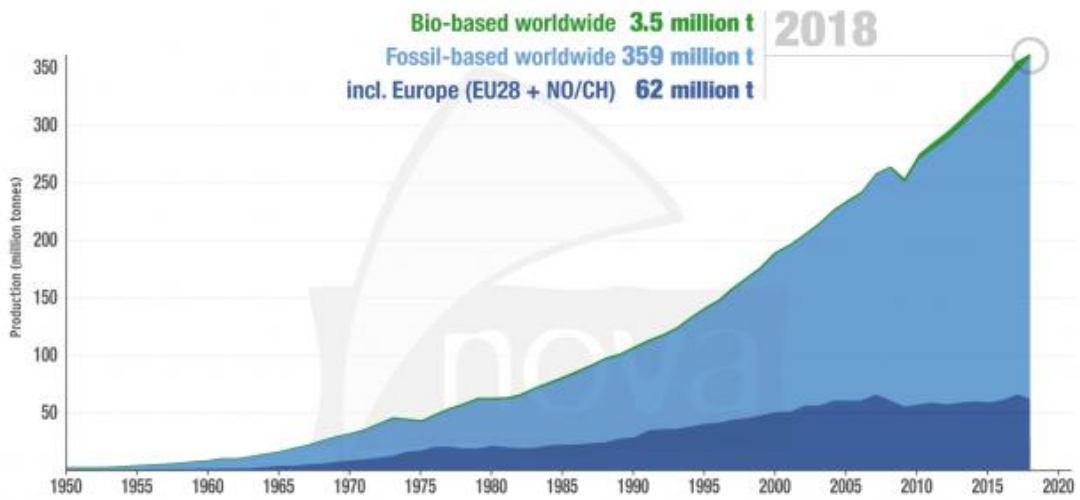


**Figure 1.2:** Global plastics production [5].

There exist many sub-groups of biopolymers, reported in Figure 1.3. A biopolymer can be:

1. bio-based and biodegradable;
2. bio-based and not biodegradable;
3. biodegradable and not bio-based.

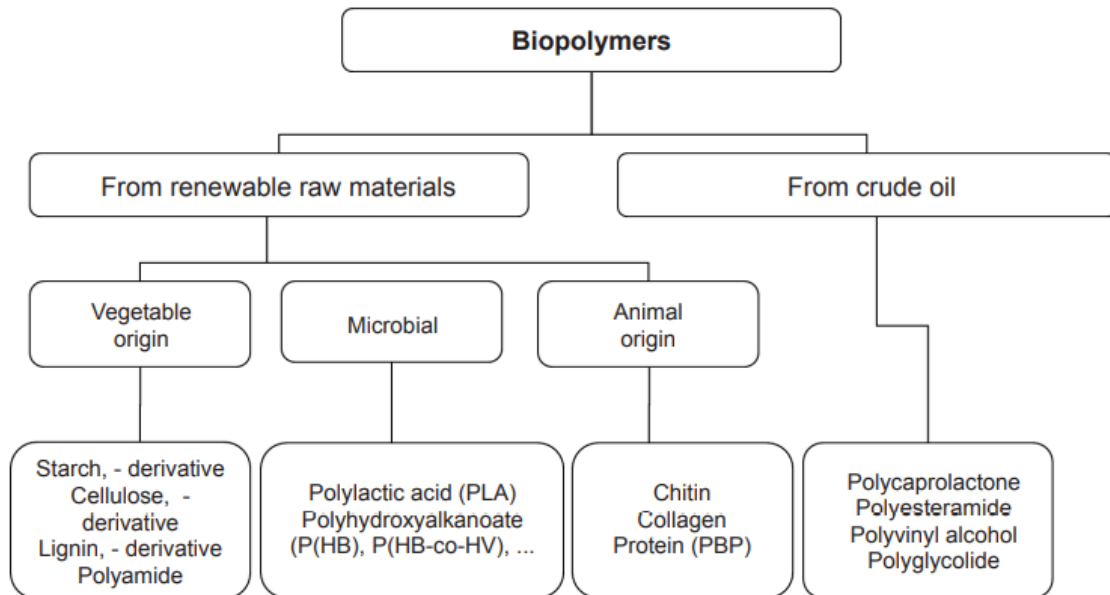


**Figure 1.3:** biopolymers classification [6].

From the 1970s many researches have tried to completely understand and to fasten the degradation reaction processes. In 1974 it was developed the first photodegradable biobased resin (1974). This resin was modified with a photosensitive additive which boost the sun photodegradation [7].

In the 1980s, the first-generation biopolymers were discovered. They consisted in a mixture of polyolefins, amide and cellulose. However, there were still some drawback since the degradation process involves the formation of dangerous microplastics. The biodegradable plastics currently produced, defined as second-generation biopolymers have improved capacity to degrade quickly. An example of these materials is constituted by polymers extracted from biomass such a maize and wheat starch. Once biodegraded, it releases small quantities of carbon dioxide into the atmosphere [7].

Maize starch was investigated in this project. There were performed two different reactions: epoxidation and methacrylation. The experiments carried out at *KTH Royal Institute of Technology* university of Stockholm (Sweden), in the *department of Fibre and Polymer Technology (FPT)*.

In the next chapter, the major polysaccharides structures and properties will be presented; followed by an overview on their most common modification mechanisms.

Then, the focus will be addressed on starch and its functionalization reactions. Particular stress will be given to the epoxidation and methacrylation reactions with an overview of the potential fields of application of the products.



## 2. State of Art

### 2.1 Polysaccharides

The isolation, synthesis and structural modification of polysaccharides and their applications, especially in *biomedical field*, are progressing rapidly and they can now be considered the most important biopolymers [8].

Polysaccharides are complex carbohydrates composed of 10 up to several thousand monosaccharides linked together forming chains. The general chemical formula for a polysaccharide is  $C_x(H_2O)_y$ . The principle examples of monosaccharides, which form the repeating units of the chain, are shown in the next Figure 2.1.

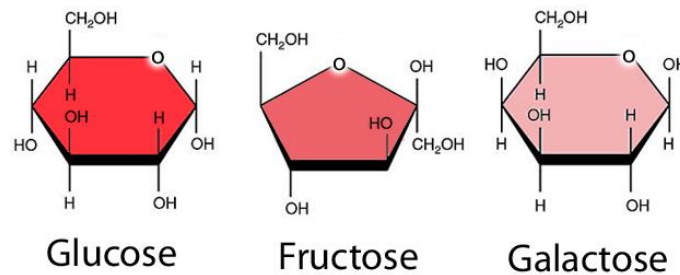


Figure 2.1: Main examples of monosaccharides [9].

Polysaccharides can be divided in two categories: *homopolysaccharides* which consist in one type of monosaccharide such as *cellulose* or *starch*, and *heteropolysaccharides* which consist of two or more different types of monosaccharides. Polysaccharides can be constituted by *homolinkages* if all the glycosidic bonds are constituted by  $\alpha$ - or  $\beta$ - configuration. Polysaccharides can also be *linear* or *branched*. Linear polysaccharides are the most abundant in nature. The average molecular weight depends on the degree of polymerization (*DP*) that is defined as the number of repetitive units present in the structure of polymers.

#### 2.1.1 Polysaccharides Functionalization

Polysaccharides are easily affordable and cheap but usually they possess poor mechanical properties. Functionalization allows to enhance them. The introduction of hydrophobic, acid, basic, or other functionality into polysaccharide structures can alter their properties. However, during the polysaccharides modification it is necessary considering some properties which make more difficult the performance of the experiments such as their ease of degradation, susceptibility to bacterial attack and interaction with some enzymes (e.g. lectin).

Figure 2.2 reports all the structural polysaccharides modifications. As reported in the scheme, there have been studied not only chemical functionalization methods but also some physical and biological techniques.

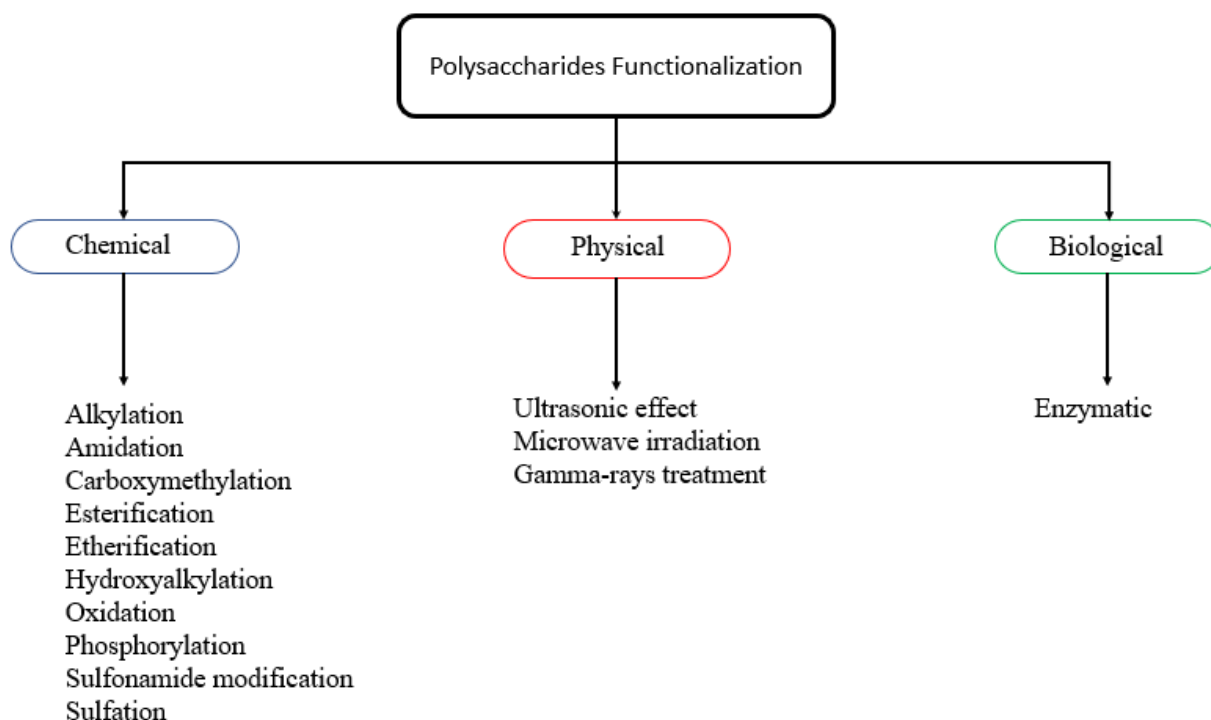


**Figure 2.2:** Polysaccharides functionalization [7].

One of the main factors when functionalization is carried out is the *regioselectivity*. This is the preference of one-direction chemical bonds that makes or breaks over all the other possible directions. However, only with monomeric molecules, when a reaction gives incomplete regioselectivity, the desired product may be purified by crystallisation or chromatography. In polysaccharides, the purification is impossible to perform because desired modified monosaccharide units are linked to undesired ones. This means that in modified polysaccharides products is often present a relevant amount of impurities [10].

## 2.2 Starch

Starch is the most important carbon reserve in plants. It is deposited in granules which are organized in crystalline and three-dimensional structures insoluble in cold water. In plants a small amount of sugar produced by photosynthesis is always stored to be secondly converted to starch. It is estimated that 60-70% of the caloric human's intake comes from starch [11].

Starch is a polysaccharide formed by the repetition of glucose hexagon rings ( $C_6H_{10}O_5$ ). It is structurally divided in two different types of macromolecules: amylose and amylopectin shown in Figure 2.3.

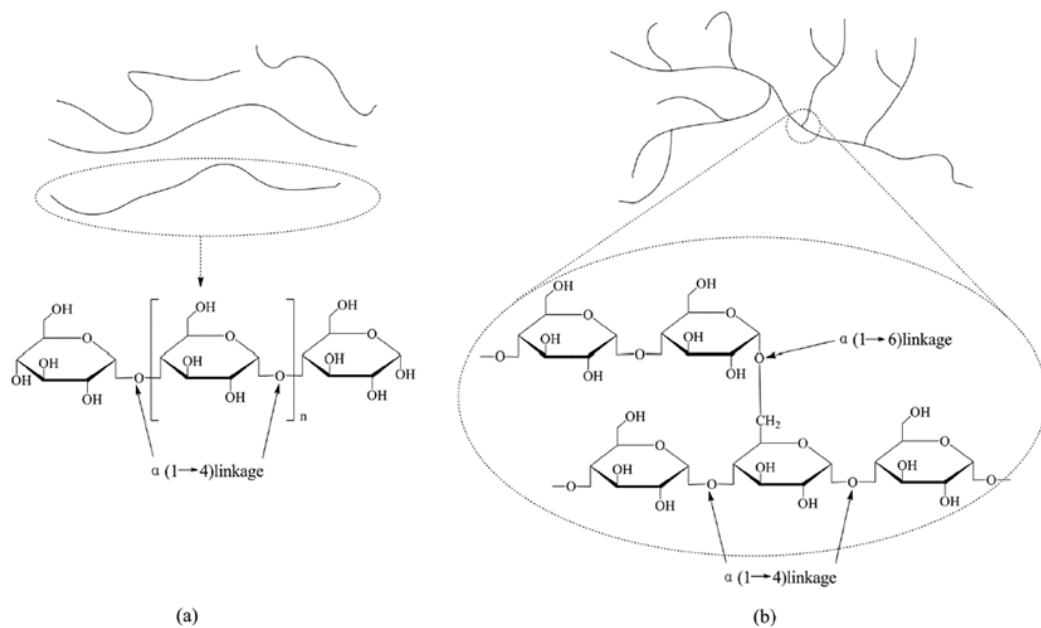


**Figure 2.3:** Chemical structures of amylose (a) and amylopectin (b) [12].

Amylose is a linear chain polymer where glycosidic units are joined together by  $\alpha$  1-4 glycosidic bonds and with a degree of polymerization (DP) of around 6000. Amylopectin is a branched chain polymer where glycosidic units are joined together by both  $\alpha$  1-4 and  $\alpha$  1-6 glycosidic bonds (branching degree from 4.2 to 5.9 %) having a DP of approximately 2 million, representing the largest molecule in nature [12]. The ratio of amylose to amylopectin varies, according to the source of starch; it ranges from 17 to 70% of amylose.

Starch granules are structurally complex systems and their dominant properties depend on the amylopectin fraction, on the DP, and on the presence of secondary components. Because of the water-insolubility of starch granules, they are easy to isolate from their plants source. The most common sources of starch are maize, beans, rice, potatoes and wheat.

## 2.2.1 Starch Biosynthesis, Gelatinization Process and Applications.

### Biosynthesis

Starch is produced enzymatically in both chloroplasts and amyloplasts. Figure 2.4 shows an example of chloroplast containing starch granules.

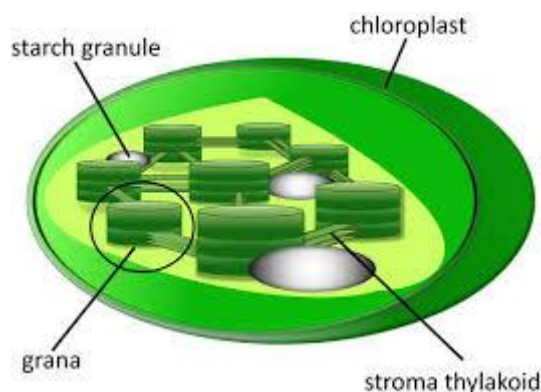


**Figure 2.4:** chloroplasts containing starch granules [13].

The starch synthesis procedure is described as follows:

1. The first step is the synthesis of ADP-glucose from glucose-1-phosphate and ATP catalysed by pyrophosphorylase (AGPase). This is the rate-determining reaction of the whole process.
2. In the second phase, ADP-glucose provides glucose for the  $\alpha$ -glucan expansion through the catalysed reaction by starch synthase. Glucose transfers from ADP-glucose to the non-reducing end of  $\alpha$ -glucan and it is responsible of amylose and amylopectin chains growth.
3. In the last step, the hydrolysis of  $\alpha$  1-4 bond and the following formation of amylopectin branching points  $\alpha$  1-6 are catalysed by starch-branching enzyme (SBE). The whole process is summarized by the following reaction mechanisms (Figure 2.5) [16].

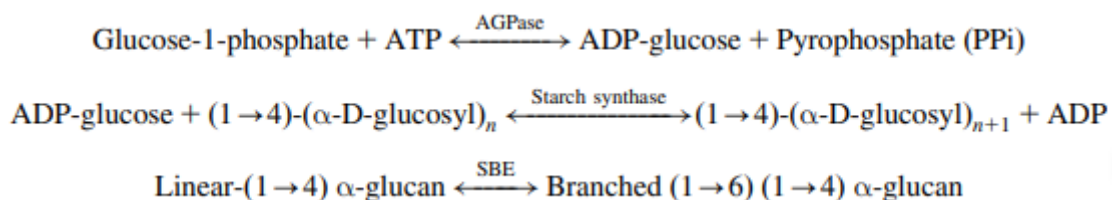


**Figure 2.5:** Starch byosynthesis mechanisms [14].

## Gelatinization

In cold water, starch granules undergo limited reversible swelling, but the integrity of the crystal structure is such that they do not dissolve. Heating the starch dispersion of granules above a characteristic gelatinisation temperature causes them to swell and form gel particles.

This process is called *gelatinization* (Figure 2.6) and it can be summarized in the following steps [15]:

1. During the warm-up, water is first absorbed into the amorphous space causing the swelling phenomenon.
2. Water then enters the areas closely related to the double helical of amylopectin. At room temperature, crystalline structures don't allow the water to get in.
3. Amylose molecules spread through surrounding water and then the grain structure disappears. These granules mostly containing amylopectin, are inside an amylose matrix forming a kind of gel.

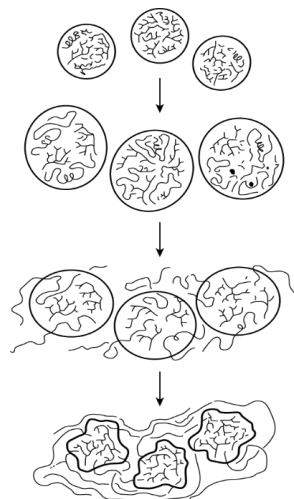


**Figure 2.6:** starch gelatinization [16]

## 2.2.2 Starch Functionalization

Chemical starch modification is carried out thanks to reactivity of functional groups present in the glycosidic units. Substitution reactions are performed with the single hydrogen atom or the hydroxide bounded with C-2, C-3 (secondary alcohol) and C-6 (primary alcohol), Most reactions with functional and multifunctional reagents give esterified and etherified starch [19].

Three main starch chemical transformations and their variations are summarized in Figure 2.7.

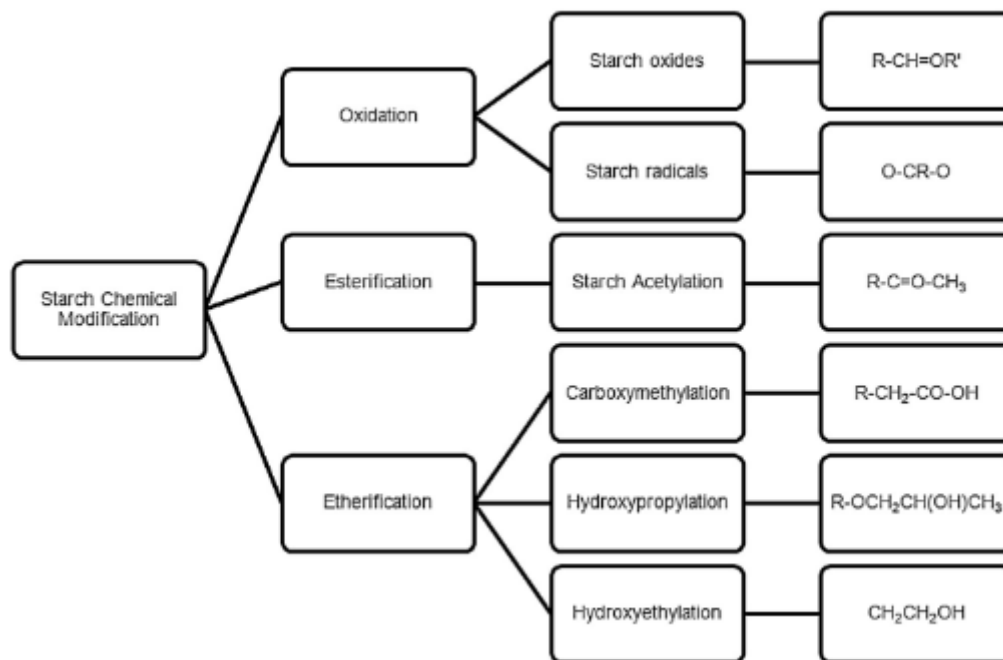


**Figure 2.7:** scheme of the main classical chemical methods for starch modification [17].

All these methods are presented in the following chapter together with the epoxidation and methacrylation reactions.

### Applications

Modified starch is commonly used in food industry. In particular it is used as a packaging of soups, sauces, pastries, milk and meat products, confectionery and snacks. Non-food starch application are pharmaceutical products, textiles, adhesives, alcohol-based fuels and biofuels. The most common industrial starch applications are reported in Figure 2.8 [18].



**Figure 2.8:** Industrial applications of starch [18].

### 2.2.2.1 Oxidation

Oxidized starch improves chemical-physical properties allowing film formation and good adhesion. The basic principle of oxidation is the starch reaction in suspension with an oxidizing agent at controlled temperature and pH. Some hydroxyl groups of glycosidic units are involved in this process to produce new derivatives products. The properties of oxidized starch depend on the nature of oxidative methods used and on the selected reagents.

Generally oxidized starch has a reduced viscosity and an improved temperature resistance, which makes it very interesting in food and pharmaceutical fields.

There are two main possible products derived by oxidative processes. One is the conversion of hydroxyl groups into carboxyl (Figure 2.9) and the other is the formation of radicals (Figure 2.10). Carboxyl groups improve the hydrophilic nature of modified starch [17].

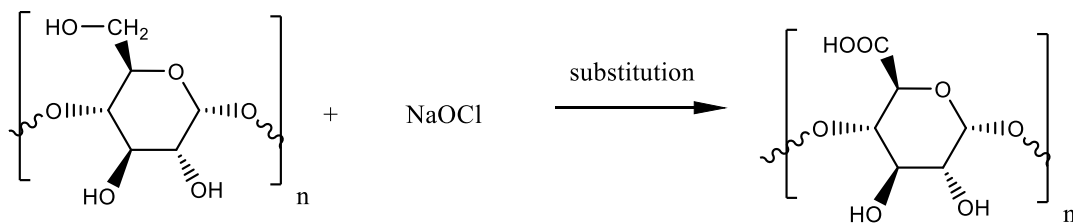


**Figure 2.9:** example of starch oxidation: carboxyl group formation

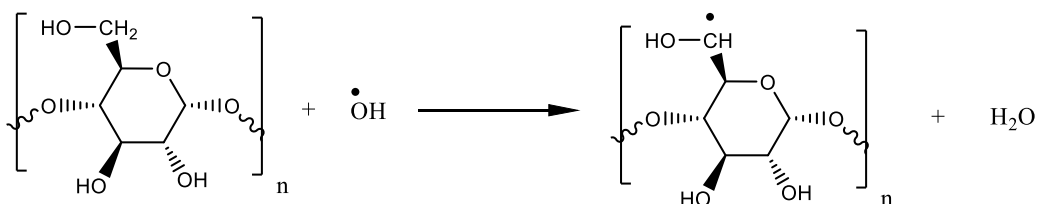


**Figure 2.10:** example of starch oxidation: radical formation

### 2.2.2.2 Esterification

There exist many different esterification methods. The most common is acetylation.[18]. There are three types of acetylated starch (Figure 2.11), based on the degree of substitution (DS).

1. Low DS starch is the most common type of acetylated starch with DS between 0.01 and 0.2 and it is soluble in cold water. To produce it, acetic anhydride is typically used as a reagent and an alkaline hydroxide such as NaOH as a catalyst.
2. Acylated Starch with an average DS between 0.3 and 1 is generally soluble in water but less than starch with low DS.
3. Acylated Starch with high DS between 2-3 is not soluble in water but it is soluble in organic solvents.

Acetyl groups ( $\text{COCH}_3$ ) have more steric hindrance than hydroxyl groups. Consequently, the electronic clouds associated with these groups are more extended. As a consequence, the chains reject each other because of steric hindrance.

This repulsion increases the swelling capacity of starch. With the increasing of DS, the reduction of starch degradation, the transition temperature ( $T_g$ ) and the gelatinization temperature become higher [21].

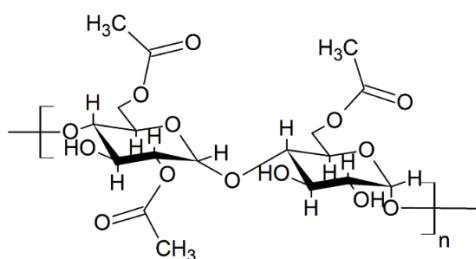


**Figure 2.11:** acetylated starch.

### 2.2.2.3 Etherification

Etherification is a method in which the hydroxyl groups are principally substituted by carboxymethyl, hydroxyethyl and hydroxypropyl ones by ether bonds ( $\text{R-OR}$ ). To perform this reaction is typically required an alkaline catalyst to initiate the chemical substitution. Etherified starch is used in drug delivery systems and as stabilizers in food industry [17].

#### Carboxymethylation

This is one of the most common methods due to its simplicity. In the next Figure 2.12 is reported the reaction involving chloroacetic acid as reagent.

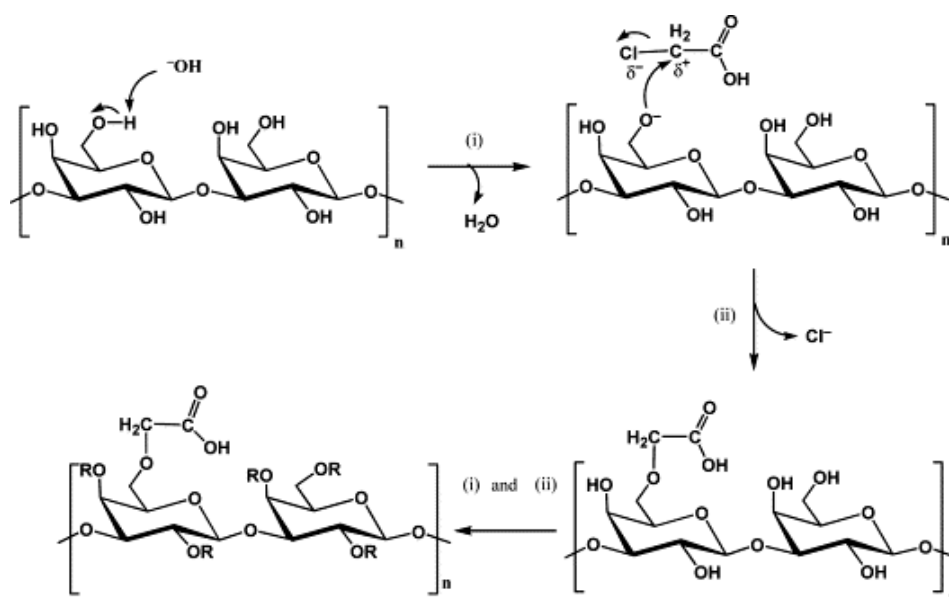


**Figure 2.12:** Starch Carboxymethylation [19].

This carboxymethyl group improves hydrophilicity and pH responsiveness [20]

### Hydroxypropylation and Hydroxyethylation

Other usual etherification methods are hydroxypropylation and hydroxyethylation, which are respectively derived using propylene oxide (Figure 2.13) and ethylene oxide (Figure 2.14) in presence of strong alkaline as catalyst.

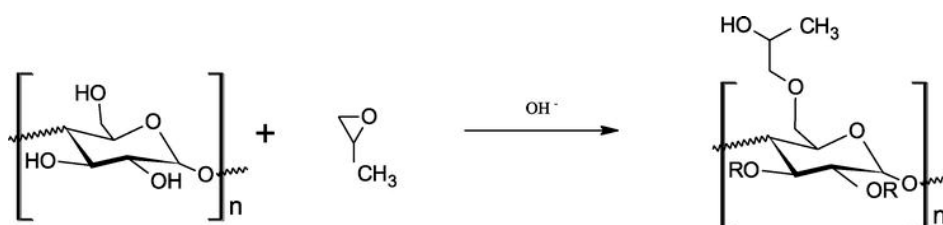


**Figure 2.13:** Etherification of starch with propylene oxide [20].

Hydroxypropyl and hydroxyethyl groups substitute the hydrogen atoms of hydroxides of the glycosidic unit. The bulky presence of these groups reduces the starch retrogradation properties. Due to the additional aliphatic chain, this molecule has also improved swelling capacity and viscosity. [23]

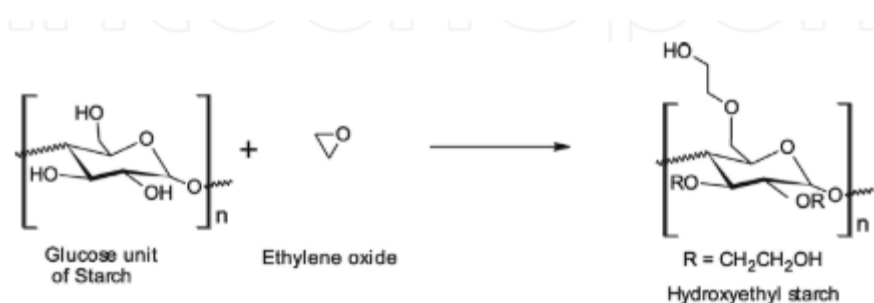


**Figure 2.14:** Etherification of starch with Ethylene oxide [20].

## 2.2.2.4 Epoxidation and Methacrylation

### Epoxidation

Epoxides are cyclic ethers structured by three ring-closed atoms to form a triangle. This triangular ring make is strained, and hence highly reactive, compared to other ethers. The basic structure is constituted by two carbon atoms linked with an oxygen one.

A reaction procedure which leads to starch epoxidation involves the use of allyl groups. Allyl groups (CH<sub>2</sub>=CH-CH<sub>2</sub>-) usually replace the hydrogen atom of hydroxyl groups of starch. Double bonds C=C of allyls are epoxidized using hydrogen peroxide (H<sub>2</sub>O<sub>2</sub>) and acetonitrile (CH<sub>3</sub>CN) in alkaline suspension. The combination of hydrogen peroxide and acetonitrile is a well-known epoxidation technique for allyl groups (Figure 2.15) [21].

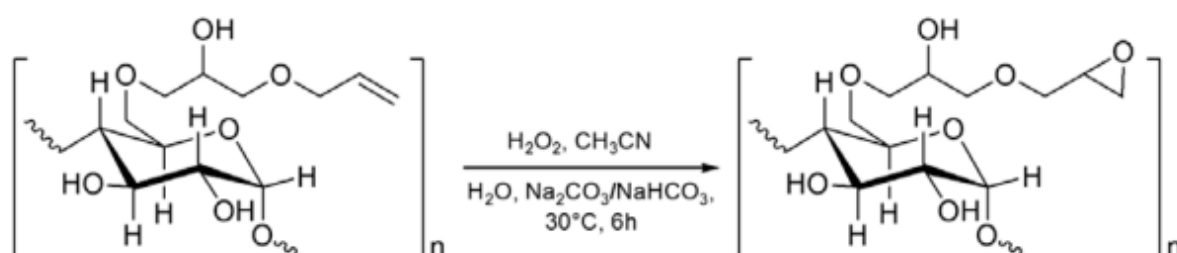


**Figure 2.15:** Allylic Starch epoxidation [21].

Epoxidation reaction often involves the use of a specific reagent, epichlorohydrin (ECH) which is a volatile, toxic, flammable epoxy compound with a sweet and pungent smell. It is mainly used in water treatment and in paper industry [22].

The industrial synthesis of ECH consists in two steps at 30 – 50 °C:

1) Reaction between allyl chloride and hypochlorous acid (Figure 2.16)

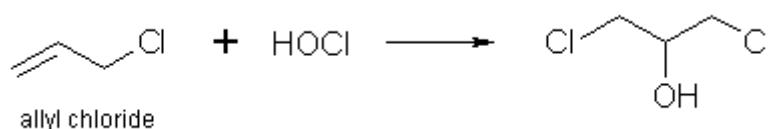


**Figure 2.16:** Addition of hypochlorous acid [23].

2) The generated dichlorohydrin is reacted with excess calcium hydroxide to form ECH (Figure 2.17)

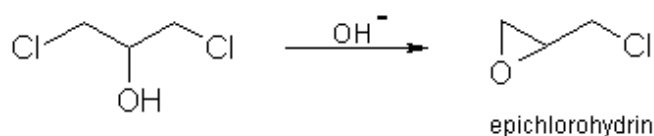


**Figure 2.17:** Reaction with calcium hydroxide [23].

Many studies were carried out concerning the interaction between starch and ECH. [24].

### Methacrylation

Chemical cross-linking of starch is proven to increase both the mechanical strength and water resistance.

In one methacrylation reaction glycidyl methacrylate (GMA) was used to obtain methacrylated starch through an epoxy ring-opening mechanism using potassium tert-butoxide as catalyst in pure DMSO (Figure 2.18) [28].

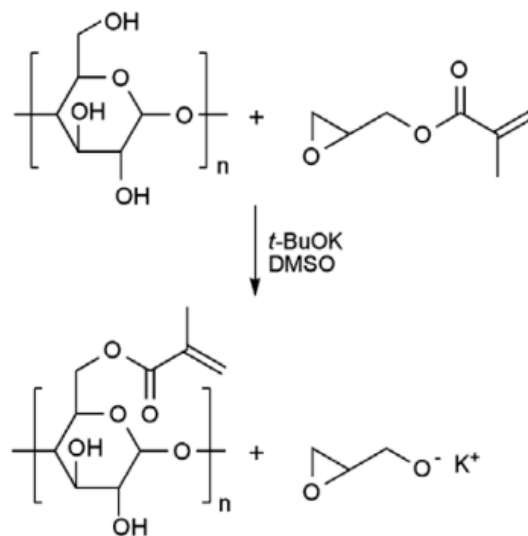


**Figure 2.18:** the reaction of starch with GMA [25].

In another study Polyethylene glycol methacrylate was used to functionalize cross-linkable hydroxyethyl starch to produce hydrogels [26].

### 2.3 Aim of the study

The purpose of this study is to investigate two different routes to functionalize native starch: epoxidation and the methacrylation.

The idea is to obtain two different types of photocurable starch derivatives.

In order to reach this goal, I spent five months in Stockholm, Sweden, at KTH Royal Institute of Technology in the fiber and polymer technology group, where I performed all the necessary experiments.

The steps followed to obtain the modified starches are:

1. Characterizing the starting high amylose maize starch by FTIR, DSC, TGA and NMR analysis.
2. Carrying out the reactions. The epichlorohydrin (ECH) was chosen as reagent of the epoxidation reaction in sodium hydroxide solution. The methacrylic anhydride was instead used as reagent of the methacrylation reaction, where starch was dissolved in pure DMSO in the presence of triethylamine.
3. Investigating the reactions products by means of FTIR-ATR, H-NMR, C-NMR and DSC analysis.



### 3. Experimental section

This chapter is focused on the materials used and the experiments performed in this project.

#### 3.1 Epoxidation reaction

##### 3.1.1 Materials

- High-amylose Hylon VII maize starch (70% amylose) obtained from Ingredion, UK.
- Distilled Water
- Sodium Hydroxide
- Epichlorohydrin (ECH)
- Ethanol absolute

##### 3.1.2 Synthesis

100 ml of distilled water was poured into a three-necked round bottom flask and approximately 1 g. of starch was added in stirring condition. The steps are shown in Figure 3.1.



**Figure 3.1:** starch weighing (a), starch and water in stirring condition (b).

The solution was gradually heated for 1 h and maintained at that temperature to gelatinize the starch. After the gelatinization was completed, the flask was equipped with both a condenser and a nitrogen inlet system to ventilate the reaction environment. Then, ECH was added dropwise at the mixture. The set-up for epoxidation reaction is shown in Figure 3.2.

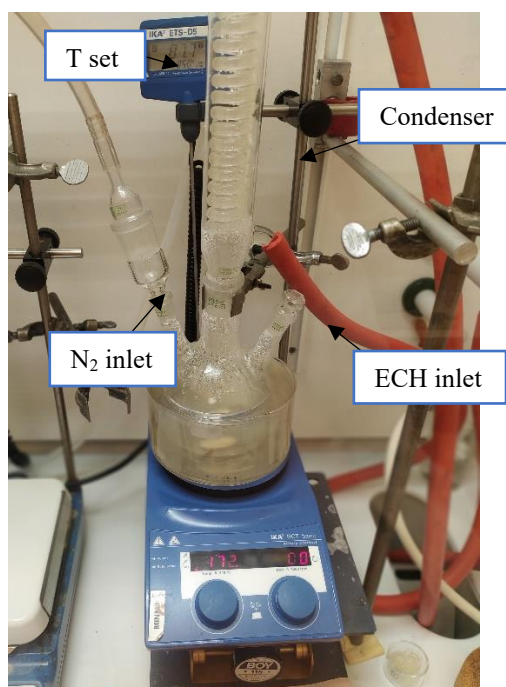


**Figure 3.2:** Experimental set-up of starch epoxidation.

The final product was precipitated and then washed with an excess of ethanol (Figure 3.3 (a)). The modified starch was firstly dried in air and then in vacuum oven. The final product appeared as a white powder (Figure 3.3 (b)).



**Figure 3.3:** washing with ethanol (a), final product (b)

The epoxidation reaction with one possible structure for epoxidized starch (EPO-Starch) is illustrated in Figure 3.4.

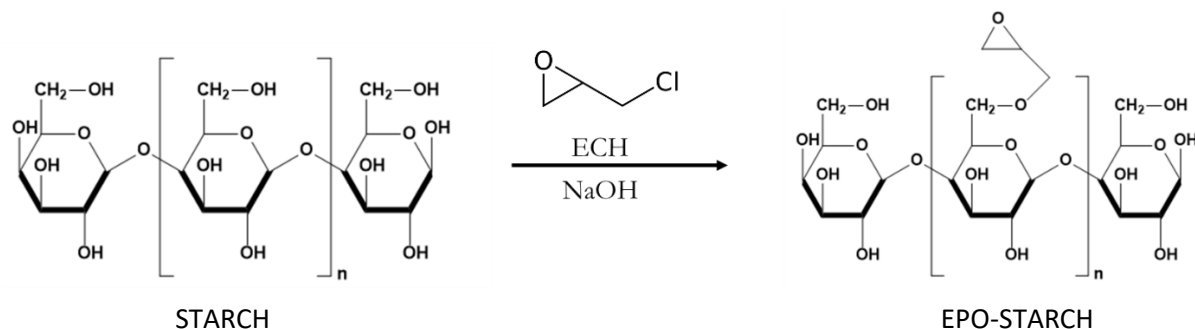


**Figure 3.4:** Schematic illustration of starch epoxidation reaction. The EPO-Starch reported structure is only one among many other possible structures and only few hydroxyl groups are substituted.

In the first five experiments, the pH was constantly monitored and kept constant at 8 by subsequent addition of sodium hydroxide. After the 5th experiment the sodium hydroxide solution was added in a fixed amount before the beginning of the reaction.

Different reaction times were taken into consideration while performing these experiments (Table 3.1).

**Table 3.1** Summary of the reaction's conditions used (1 to 8).

Reaction	Starch [g]	ECH [ml]	Molar ratio (ECH: <sup>1</sup> AGU:NaOH)	NaOH Solution [ml]	Time [h]	Temperature [°C]
ES-1	1.00	0.48	1:1: -	undefined	2	85
ES-2	1.03	1.00	2:1: -	undefined	2	85
ES-3	1.01	1.47	3:1: -	undefined	2	85
ES-4	1.03	2.49	5:1: -	undefined	2	85
ES-5	1.07	0.52	1:1: -	undefined	2	100
ES-6	1.04	3.52	7:1:1	12.83	5	85
ES-7	1.10	3.74	7:1:1	13.62	5	85
ES-8	1.10	6.39	12:1:1	13.58	5	85

<sup>1</sup>AGU: anhydroglucose unit

From the reaction 9 to 12 (Table 3.2), the main difference was the direct using of a fixed amount of 0.5 M NaOH solution at the beginning of the experiment instead of distilled water.

**Table 3.2:** Summary of the reaction's conditions used (9 to 12).

<b>Reaction</b>	<b>Starch [g]</b>	<b>ECH [ml]</b>	<b>Molar ratio (ECH:AGU:NaOH)</b>	<b>NaOH Solution [ml]</b>	<b>Time [h]</b>	<b>Temperature [°C]</b>
<b>ES-9</b>	1.16	6.70	12:1:12	<b>171.85</b>	5	85
<b>ES-10</b>	1.06	7,79	<b>15:1:15</b>	196	5	85
<b>ES-11</b>	1.05	8,64	<b>17:1:17</b>	220	5	85
<b>ES-12</b>	1.02	9,87	<b>20:1:20</b>	251,8	5	85

## 3.2 Methacrylation Reaction

### 3.2.1 Materials

- High-amylose Hylon VII maize starch (70% amylose) obtained from Ingredion, UK
- Methacrylic anhydride-MA
- Triethylamine-TEA (>99%)
- Dimethyl sulfoxide-DMSO (ACS reagent >99.9%)
- Ethanol absolute

### 3.2.2 Synthesis

Maize starch and DMSO were placed in a round-bottom flask under stirring condition (6 g of maize starch in 200 ml DMSO). The temperature was then increased to 70°C. After 30 minutes the starch had been gelatinized and the solution was cooled down to room temperature. Methacrylic anhydride was then added dropwise with a syringe and triethylamine, as a nucleophilic catalyst, was added slowly. (molar ratio AGU:MA:TEA of 1:2:0.04). The final solution was kept at room temperature for 18 h.

After 18 h the product was precipitated in ethanol, dissolved in deionized water and again precipitated in ethanol. This procedure was repeated two times in order to purify the product. The final aqueous solution was lyophilized.

The main steps of the starch methacrylation are reported in the Figure 3.3.



**Figure 3.3:** Main steps of the starch methacrylation reaction. From the left: starch dissolution in DMSO (a), MA-starch reaction end (b), MA-starch precipitation (c), lyophilized product (d)

The methacrylation reaction with one possible structure for methacrylated starch (MA-Starch) is illustrated in Figure 3.4.

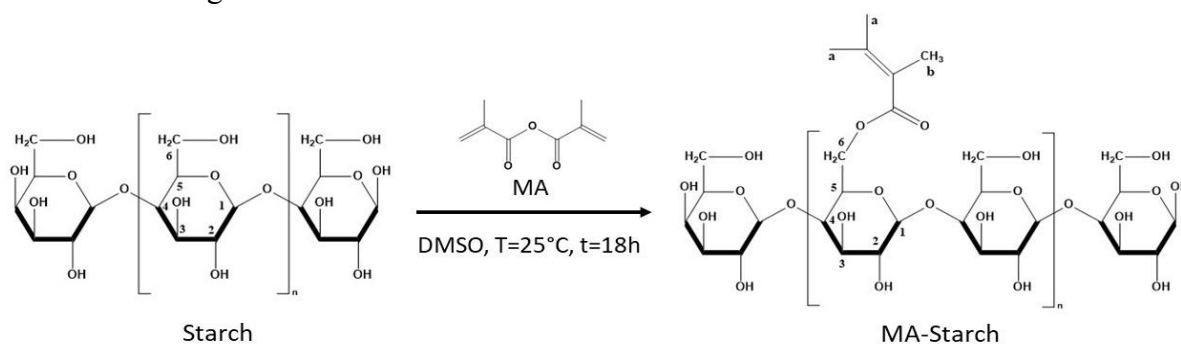


**Figure 3.4:** Schematic illustration of starch methacrylation reaction. The MA-Starch reported structure is only one among many other possible structures and only few hydroxyl groups are substituted.

## 4. Methods

In this chapter, different characterization techniques used to investigate starch and starch derivatives are described. It will be firstly given an overview on instruments working principles and then it will be provided the experimental conditions applied.

The reaction products were examined by means of proton nuclear magnetic resonance ( $^1\text{H}$ -NMR), carbon nuclear magnetic resonance ( $^{13}\text{C}$ -NMR), attenuated total reflectance – Fourier transform infrared (ATR-FTIR) spectroscopy, differential scanning calorimetry (DSC) and thermogravimetric analysis (TGA).

### 4.1 Nuclear magnetic resonance (NMR)

Nuclear Magnetic Resonance (NMR) is an instrumental analytic technique which allows to obtain detailed information on the molecular structure by observing the behaviour of atomic nuclei in a magnetic field.

The nuclei of many elemental isotopes have a characteristic spin ( $I$ ). Some nuclei have integrals spins, some have fractional spin, and a few have no spin. The isotopes treated in this project ( $^1\text{H}$  and  $^{13}\text{C}$ ) have  $I=1/2$ .

A spinning charge generates a magnetic field ( $B_0$ ). The resulting spin-magnet has a magnetic moment ( $\mu$ ) proportional to the spin. In absence of magnetic field nuclear spins are randomly oriented, while, in presence of an external field, two spin states exist:  $\alpha$  ( $+1/2$ ) and  $\beta$  ( $-1/2$ ). The first is at lower energy and is aligned with the external magnetic field, while the second is at higher energy and opposed to the external magnetic field. The energy difference is always small and depends on the strength of the magnetic field. The following Figure 4.1 shows the splitting of nuclei spin energies when a magnetic field is applied. It's clear that two spin states have the same energy ( $\Delta E = 0$ ) when the external field is zero but grows as the field increases

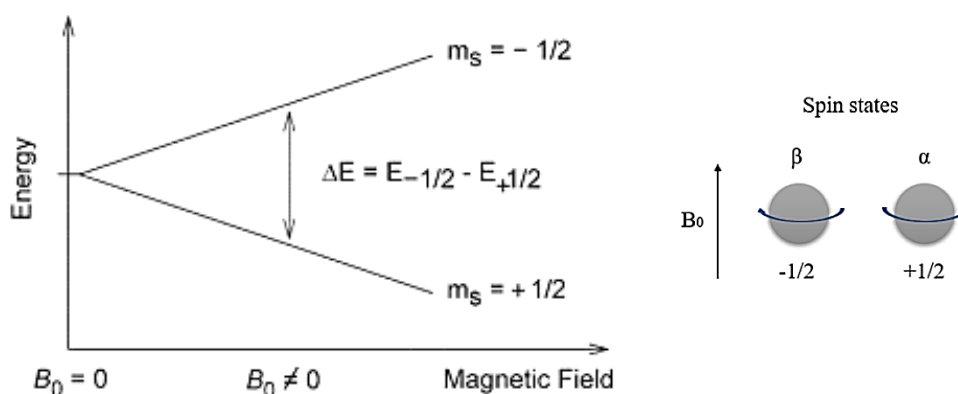


**Figure 4.1:** Difference between the two spin states and the external magnetic field

For NMR this energy difference is given as a frequency between 20 and 900 MHz, depending on the magnetic field applied and nuclei investigated.

The following equation 4.1 shows the linear correlation between frequency and nucleus momentum

$$\nu = \frac{\mu B_0}{hI} \quad (4.1)$$

Where:

- $\nu$ : frequency [MHz];
- $\mu$ : Magnetic moment;
- $B_0$ : External magnetic field;
- $h$ : Plank's constant ( $6.626 \cdot 10^{-34}$  [J·s]);
- $I$ : spin ( $+\frac{1}{2}$  or  $-\frac{1}{2}$ ).

The difference between the two energy levels is given by the following equation 4.2.

$$\Delta E = h\nu \quad (4.2)$$

### 5.1.1 Proton nuclear magnetic resonance ( $^1\text{H}$ -NMR)

Many protons  $^1\text{H}$  are non-equivalent in many compounds because they create different magnetic fields and signal in  $^1\text{H}$ -NMR spectra.

To begin with the analysis, the NMR spectrometer must be set to a specific nucleus, the proton in this case. The sample solution is poured in a uniform glass tube, oriented between the poles of a powerful magnet and centrifugated to average the magnetic field variations. The radiofrequency is broadcast into the sample from a coil. Another coil receives the energy emissions which are monitored by a computer. This signal is reported in a graph called spectrum, where on the x-axis the chemical shifts ( $\delta$ ) is measured in ppm and on the y-axis, there is the signal strength.

Chemical shift is calculated using a proton of tetramethylsilane ( $(\text{CH}_3)_4\text{Si}$ ), set at 0.00 ppm, as a reference.

The NMR apparatus, the glass tube and the scheme of the process are shown in the following Figure 4.2.

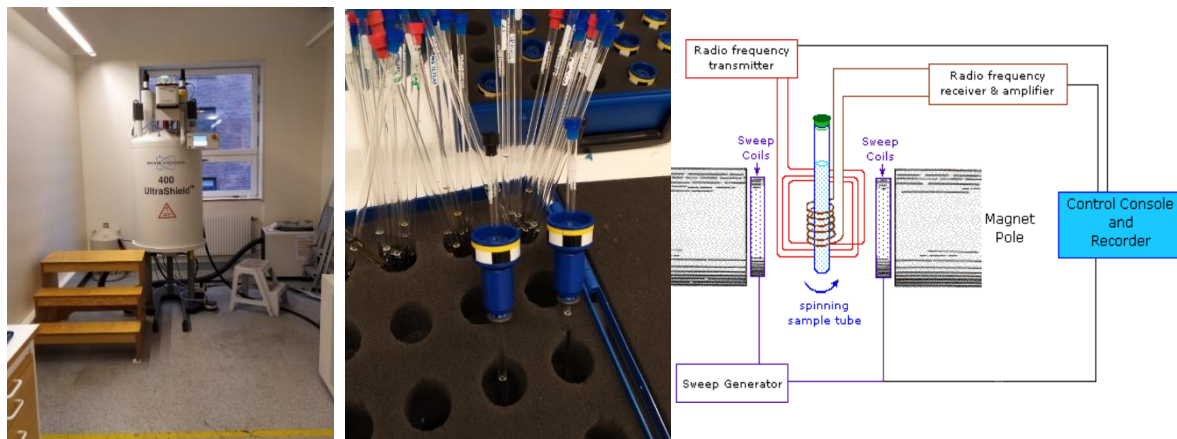


**Figure 4.2:** From the left: NMR apparatus (a), glass tubes (b), process (c) [27].

In this work,  $^1\text{H}$ -NMR was performed in order to characterize native and modified starches.

Native starch, EPO-Starch and MA-Starch were analysed by Bruker Advance 400 Fourier Transform NMR spectrometer (FT-NMR) operating at 400 MHz, at room temperature. The glass tubes were filled with about 8 mg/ml of modified starch in DMSO-d<sub>6</sub>. The MestReNova software was used to analyse and compare the results.

#### 4.1.2 Carbon nuclear magnetic resonance ( $^{13}\text{C}$ -NMR)

The principles of  $^{13}\text{C}$ -NMR are essentially the same of  $^1\text{H}$ -NMR, but there are several differences.

This analysis allows to determine the carbon atoms in an organic molecule as  $^1\text{H}$ -NMR identifies hydrogen atoms.

The main carbon isotope,  $^{12}\text{C}$  has a zero-spin quantum number and then it is not magnetically active and not detectable by NMR. For this reason,  $^{13}\text{C}$ -NMR detects only  $^{13}\text{C}$  carbon isotope which represent only the 1.1% of elemental carbon and it is magnetically active because has  $I = \frac{1}{2}$ .

Therefore, there is a low instrumental sensitivity, which determines a low value of the signal/noise ratio (S/N). One of the solutions of this problem is given by the instrumental technique FT/NMR, which allows to amplify the spectrum  $n$  times ( $n=2, 4, 8, 16$  and so on). This cause a lower noise, with consequent increase of S/N ( $S/N=n^{1/2}$ ). [28]

Unlike the  $^1\text{H}$ -NMR spectrum, the relative  $^{13}\text{C}$ -NMR signal strength is not directly proportional to the number of present carbon atoms, accordingly the integral does not provide any information. Therefore, the number of signals and their chemical shifts give the most important information.

The apparatus is the same of the  $^1\text{H}$ -NMR analysis and it is shown in the previous Figure 4.2.

In this work,  $^{13}\text{C}$ -NMR was used to characterize the product of the methacrylation reaction, in order to confirm the substitution of the hydroxyl group by methacrylated one onto the starch structure.

The tests were conducted at 60°C with 20 mg/ml of starch in DMSO-d<sub>6</sub>.

#### 4.2 Attenuated Total Reflectance – Fourier transform infrared (ATR-FTIR) spectroscopy

Attenuated Total Reflection Fourier Transform IR Spectroscopy (ATR-FTIR) is an analytical technique that is based on the interaction between the electromagnetic vibration and the material. Unlike the traditional Fourier Transform Infrared Spectroscopy (FTIR), ATR allows to examine solid and liquid samples easily.

ATR uses the properties of the evanescent wave in total reflection. The sample is first placed in contact with an optical dense element called internal reflection element (or ATR crystal) marked by high refractive index. The IR beam emitted is sent to the surface of the ATR crystal, then it enters the crystal, it is reflected through the crystal and penetrates inside the sample being partially absorbed.

After some reflections, the intensity of IR beam is enough to be detected by the spectrophotometer.

The working principle is presented in the following Figure 4.3.

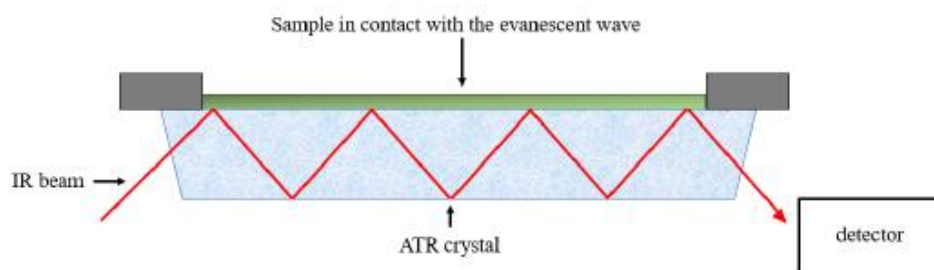


**Figure 4.3:** Schematic representation of ATR-FTIR working principle.

When a molecule is hit with specific IR frequency ( $\nu$ ) radiation (expressed as a wave number  $1/\lambda$ , in  $\text{cm}^{-1}$ ), the energy is converted into rotational and vibrational motions. The variations occurring in the IR beam are due to the alteration of the evanescent wave and depend on the type of material since different chemical bonds absorb in different region.

In the electromagnetic spectrum, infrared region is located between the visible and microwave regions (Figure 4.4).

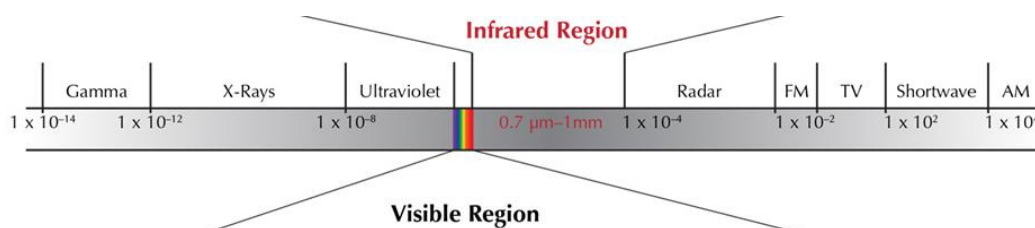


**Figure 4.4:** Evidence of Infrared Region [29].

In this work, ATR-FTIR was carried out in order to characterize native and modified starches. The tests were performed using a Perkin-Elmer Spectrum 2000 (16 scans, resolution  $4 \text{ cm}^{-1}$ ). The ATR-FTIR apparatus used is shown in Figure 4.5.



**Figure 4.5:** ATR-FTIR instrumental apparatus

### 4.3 Differential scanning calorimetry (DSC)

Differential scanning calorimetry (DSC) is a thermal analysis technique used to measure temperature and heat flow associated with the transitions that occur in a sample such as melting, crystallization and glass transition temperature. This technique allows to obtain material information by heating or cooling it in a controlled way. The energy is introduced into a furnace containing the sample and the reference pans. The sensors are connected to thermocouples allowing to record the temperature difference. Accordingly, during the whole test both the sample and the reference are kept at the same the temperature increasing it linearly. The physical transitions are recorded and reported in a thermogram, showing the temperature on x-axis and the heat flow variations on y-axis.

A schematic representation of DSC instrument is shown in the following Figure 4.6.

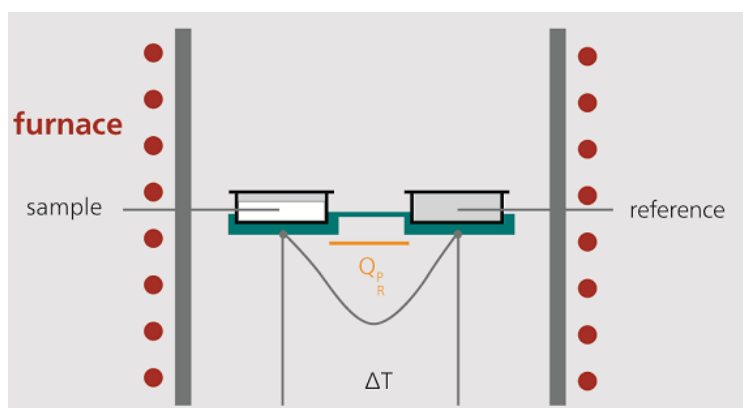


**Figure 4.6:** Scheme of a DSC measurement chamber [30].

DSC was used in this work to evaluate the thermal transition of the functionalized polymers comparing them to the starting starch. The measurements were carried out using a DSC Mettler Toledo DSC 820. Samples having masses of approximately 7 mg were insert in a 100  $\mu\text{l}$  aluminium pans with pierced lids. The applied heating rate was 10  $^{\circ}\text{C min}^{-1}$  in a nitrogen atmosphere (rate 50  $\mu\text{l/min}$ ). Thermal behaviour of the samples was investigated using the following heating-cooling cycles: the temperature was raised from room temperature to 100  $^{\circ}\text{C}$ , then cooled down to -30 $^{\circ}\text{C}$  and raised again to 200 $^{\circ}\text{C}$ . The glass transition temperature ( $T_g$ ) was determined from the second heating curve.

The DSC apparatus used for the characterization of the polymers is shown in Figure 4.7.

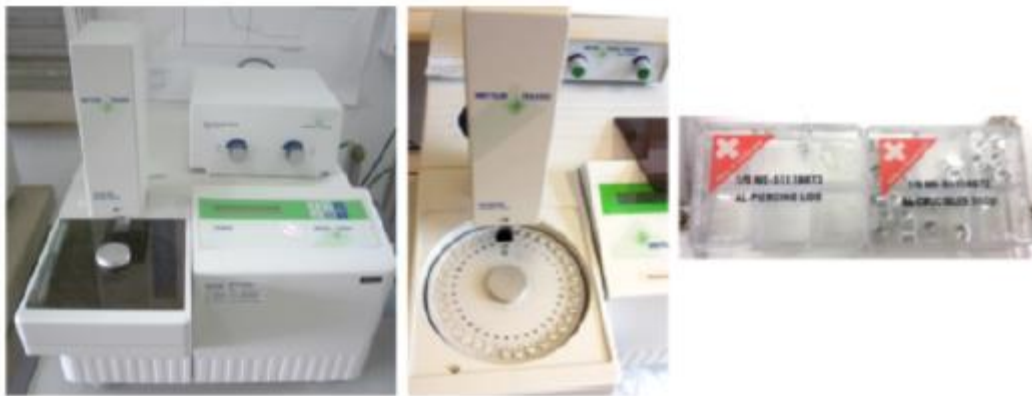


**Figure 4.7:** DSC apparatus

#### 4.4 Thermogravimetric analysis (TGA)

Thermogravimetric analysis (TGA) is a thermal analysis used to monitor the weight variations of the sample upon heating as a function of temperature or time. The measurement is carried out in air or inert atmosphere such as nitrogen. In some cases, the measurements are carried out with low oxygen content (1 to 5% w/w) in order to slow down any oxidation reactions.

TGA can detect different physical processes, such as phase transitions or chemical processes like chemisorption and decomposition. This is a quantitative analytical technique which does not provide indications on the sample nature.

In Figure 4.8 is shown the chamber where is carried out the measurement. The sample is inserted within a crucible that is positioned onto a precision micro-balance.

The atmosphere and the heating rate are precisely monitored during the whole analysis.

The results are finally reported in a thermogravimetric graph in which the % of weight loss is on the y-axis and the temperature (or time) is on the x-axis.

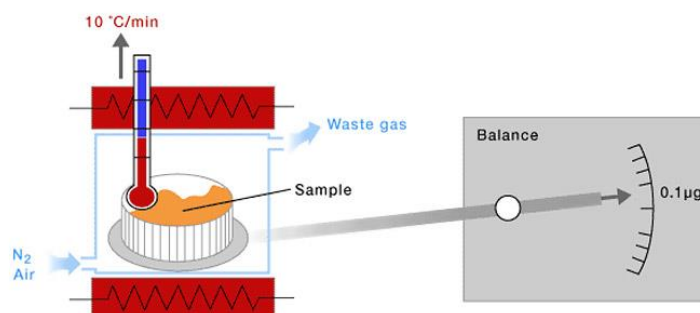


**Figure 4.8:** Schematic representation of TGA measurement chamber [31].

TGA was used in this study to investigate the thermal stability of native starch as compared to that of EPO-starch. The samples were placed in alumina crucibles (70  $\mu$ L) that were used without lids. The tests were run from 15°C to 800°C under nitrogen flux, using a TGA Mettler Toledo (USA). The results were analysed using STARe software.

The TGA apparatus used for the characterization of polymers is shown in the following Figure 4.9.

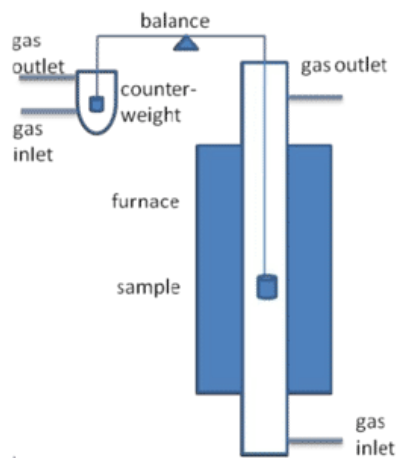


**Figure 4.9:** Schematic representation of TGA measurement chamber [32].

## 5. Results and discussion

The results of the characterization analysis described in the previous chapter 4 are discussed here below.

In the first section, the molecular structure of high amylose maize starch is characterized. In the second and third sections, comparisons between the starting material and the obtained products is provided.

### 5.1 Maize starch characterization

High amylose maize starch was characterized by the ATR-FTIR,  $^1\text{H-NMR}$ , DSC and TGA techniques.

#### 5.1.1 ATR-FTIR analysis

FTIR analysis was performed on the native starch sample, in order to determine the structure of the molecule. The results are shown in Figure 5.1.

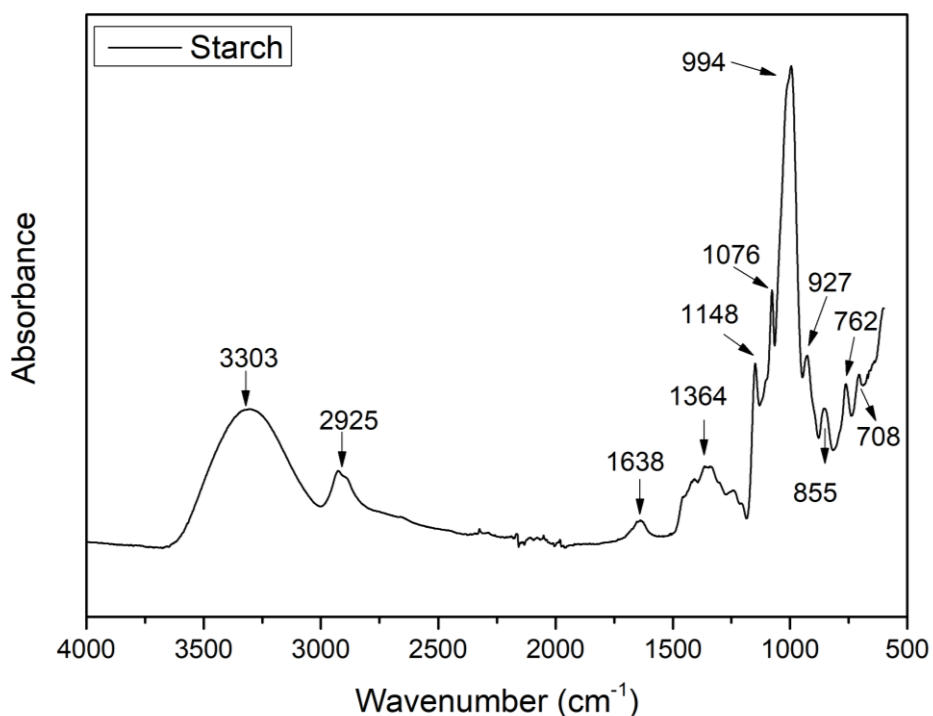


**Figure 5.1:** FTIR spectrum of maize starch

In the Table 5.1 are summarized the types of bond to the respective peaks.

**Table 5.1:** FTIR starch spectrum analysis.

BAND	TYPE OF BOND
3303 $cm^{-1}$	Stretching vibration of strong band of hydroxyl groups [34]
2925 $cm^{-1}$	Deformation vibration of C-H [34]
1638 $cm^{-1}$	Deformation vibration hydroxyl group of H <sub>2</sub> O absorbed in the amorphous region of starch [35]
1364 $cm^{-1}$	C-H <sub>2</sub> bending modes [33]
1148 $cm^{-1}$	C-O-C symmetric stretching of cyclic ether group [34]
1076 $cm^{-1}$	Bending vibration of C-H [34]
994 $cm^{-1}$	Stretching vibration of C-O-C [34]
927 $cm^{-1}$	Skeleton vibration of C-O-C $\alpha$ 1-4 glycosidic linkages [33]
855 $cm^{-1}$	C[1]-H, CH <sub>2</sub> (deformation) [34]
762 $cm^{-1}$	C-C (stretching) [33]

### 5.1.2 <sup>1</sup>H-NMR analysis

Proton nuclear magnetic resonance analysis was performed on native starch, in order to determine the structure of the molecule. The solvent for NMR analysis was prepared by mixing 8 grams of starch with 1 ml of pure DMSO, dissolved using a shaking table.

The result is shown in Figure 5.2.

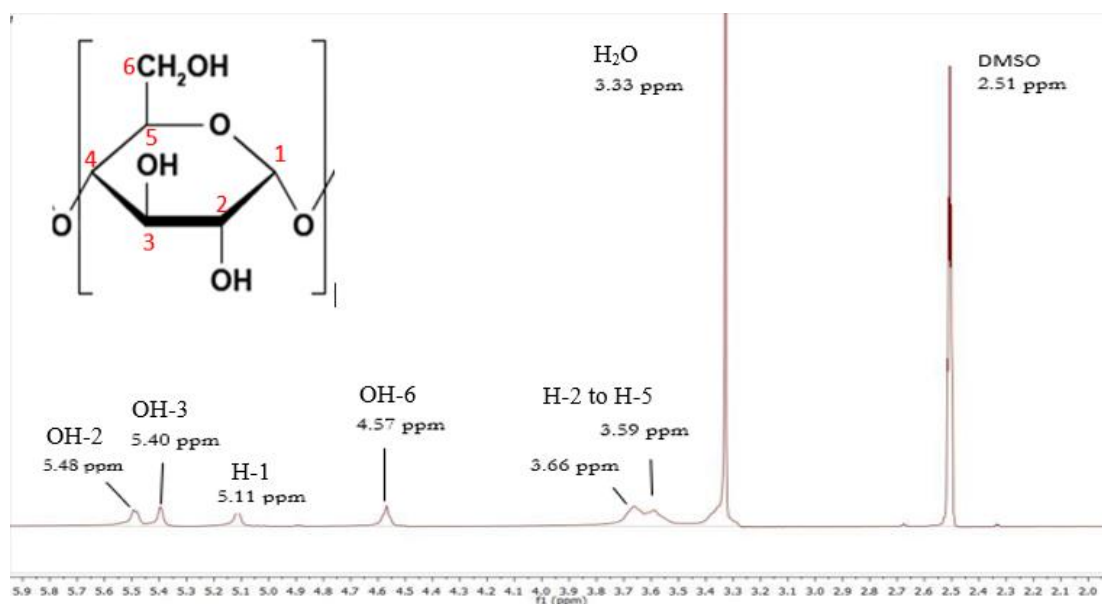


**Figure 5.2** <sup>1</sup>H-NMR spectrum of maize starch.

### 5.1.3 $^{13}\text{C}$ -NMR analysis

The  $^{13}\text{C}$ -NMR of starch is reported in the Figure 5.3. All the carbon atoms of the starch repeating unit can be detected and assigned. The signals at 100.54, 79.37, 73.74, 72.55, 72.12 and 61.09 ppm can be attributed to C1, C4, C3, C2, C5 and C6 of the anhydrous glucose unit respectively [50].

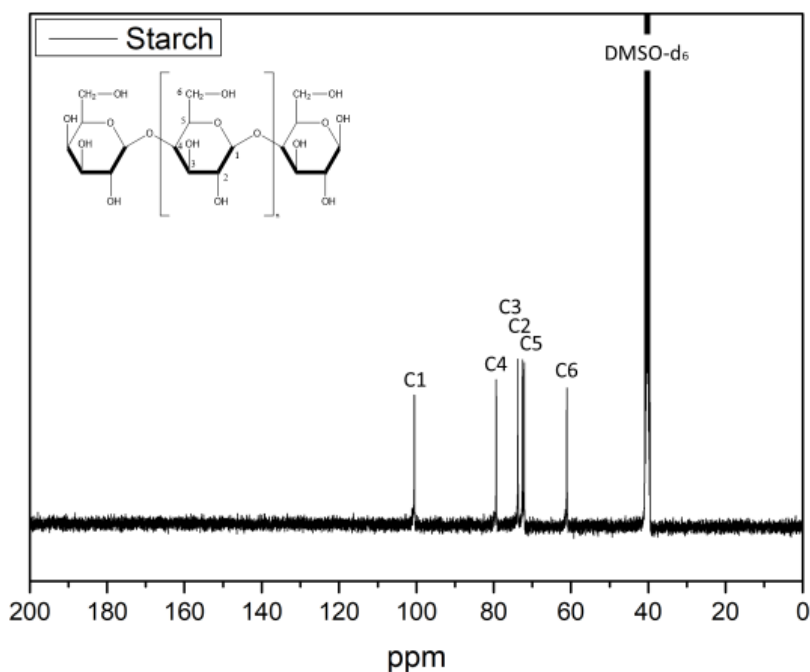


Figure 5.3:  $^{13}\text{C}$ -NMR spectrum of maize starch [50].

### 5.1.4 DSC analysis

DSC analysis shown in Figure 5.4 was performed on the maize starch sample, in order to determine the glass transition temperature ( $T_g$ ). This was measured through the average of three samples and equal to 107 °C (st. dev.= 2.9 °C).

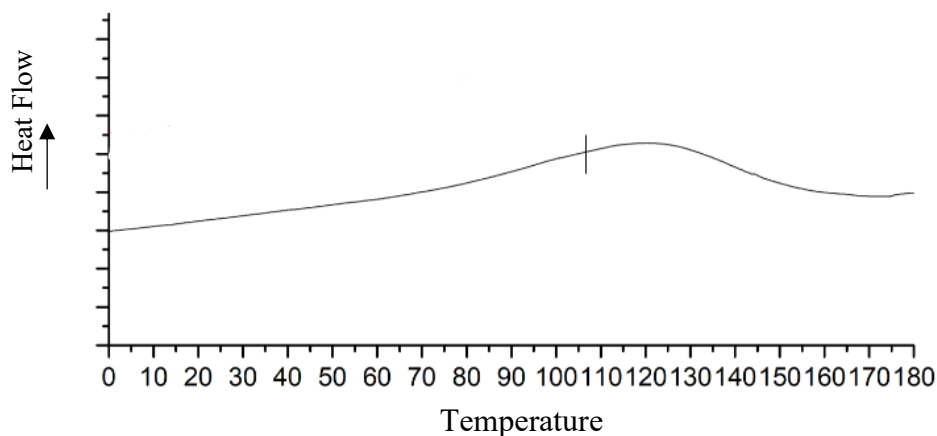


Figure 5.4: DSC analysis on native starch sample

### 5.1.5 TGA analysis

Thermogravimetric analysis shown in Figure 5.5 is performed to determine thermal stability of maize starch and its fraction of volatile components by monitoring the weight change that occurs while heating. The percentage of volatile component is 4.5% by weight. The starch degradation starts at around 250 °C. The temperature of the maximum weight loss rate  $T_0 = dm/dT_{\max}$  is 309,9 °C. The residual mass  $M_{\text{res}}$  at 700°C is 15.8%.

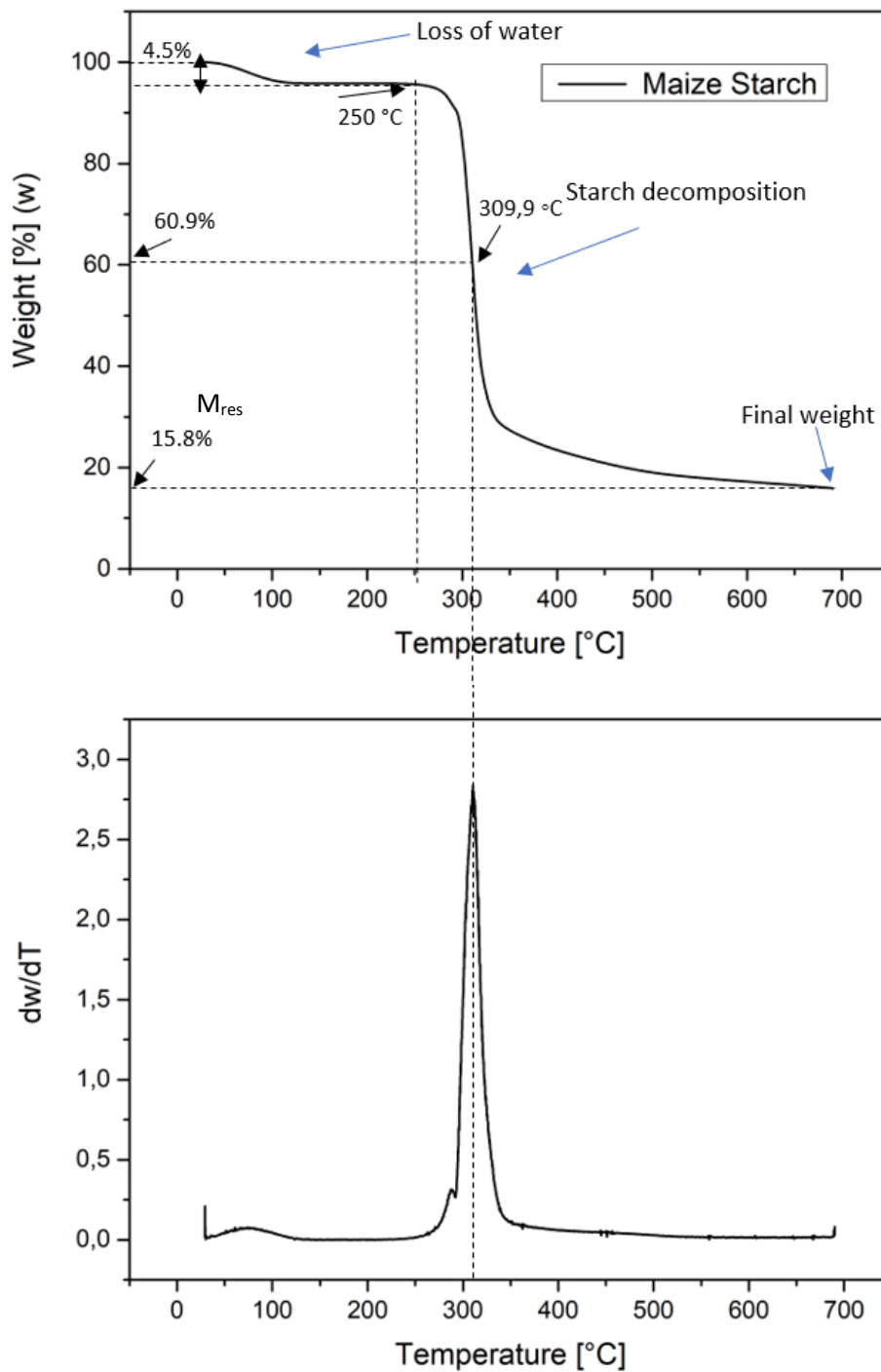


Figure 5.5: TGA of maize starch

## 5.2 Epoxidation Reaction

### 5.2.1 ES-1, ES-2, ES-3 analysis

The reactions will be examined chronologically in the following paragraphs. The first three reaction conditions are presented in the Table 5.2. The products obtained after these experiments are compared with native starch.

**Table 5.2:** experimental parameters for ES-1, ES-2 and ES-3.

Reaction	Starch [g]	ECH [ml]	Molar ratio (ECH:AGU:NaOH)	NaOH Solution [ml]	Time [h]	Temperature [°C]
ES-1	1.00	0.48	1:1: -	undefined	2	85
ES-2	1.03	1.00	2:1: -	undefined	2	85
ES-3	1.01	1.47	3:1: -	undefined	2	85

There are no appreciable differences between the spectra reported in Figure 5.6 concerning the number of peaks. However, since the epoxy ring and ether bond peaks [34] can be partially overlapped by C-H and C-H<sub>2</sub> vibrations respectively, it was decided to analyse and compare the integrals of these peaks before and after the epoxidation reaction.

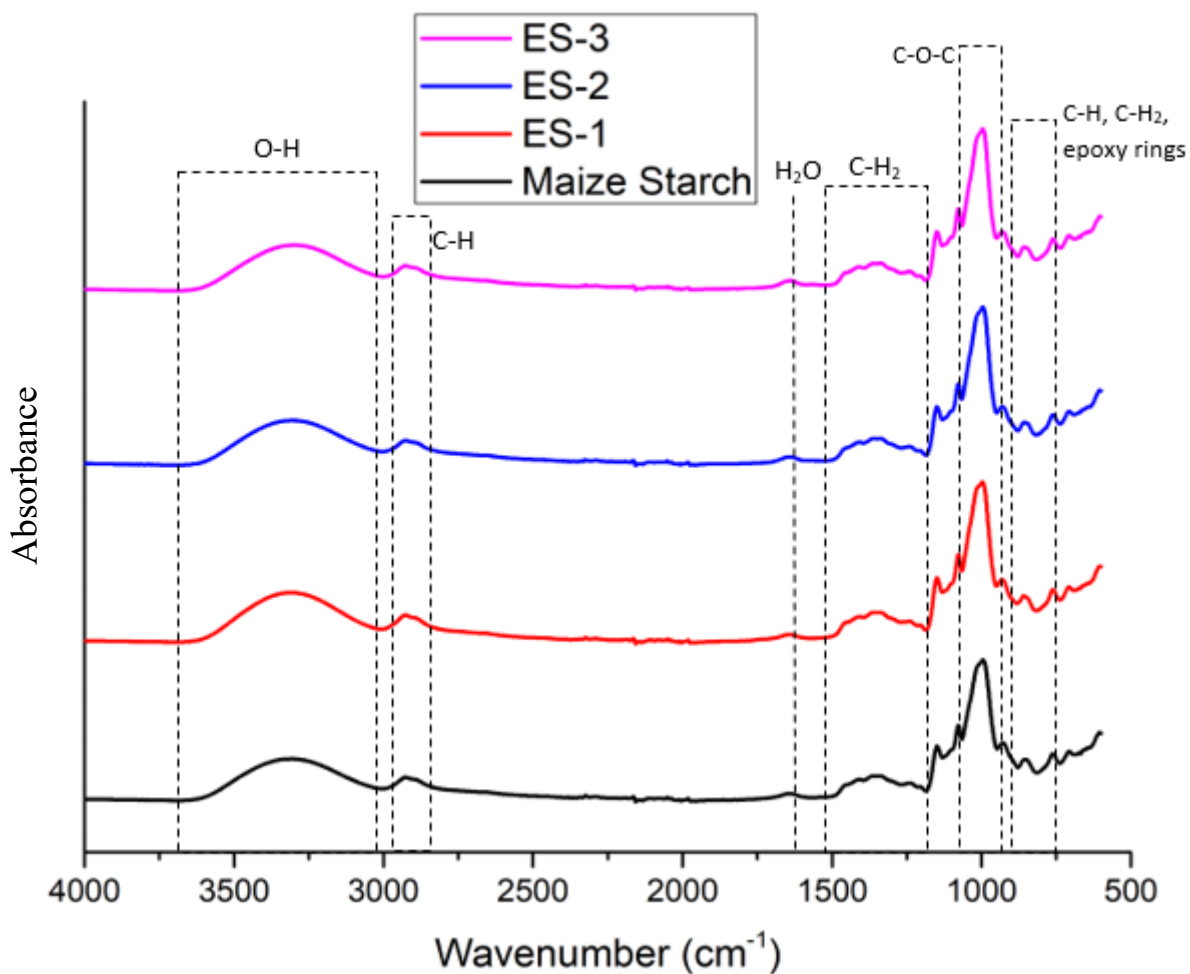


**Figure 5.6:** FTIR spectra of maize starch and modified starches ES-1, ES-2, ES-3.

The following Table 5.3 shows the normalized areas of the peaks previously described. The area chosen as a reference to normalize the peaks was  $[3303 - 2800 \text{ cm}^{-1}]$ , which can be attributed to C-H deformation vibration. The results show a slight increase of the areas of the peaks along with the increase of ECH amount, except for the ES-1 reaction.

**Table 5.3:** Normalized areas comparison between Maize starch, ES-1, ES-2 and ES-3 reactions.

	Normalized Area $994 \text{ cm}^{-1}$	Normalized Area $855 \text{ cm}^{-1}$
<b>Maize starch</b>	5.15	0.30
<b>ES-1</b>	4.69	0.25
<b>ES-2</b>	6.00	0.30
<b>ES-3</b>	6.23	0.33

The Figure 5.7 shows the  $^1\text{H}$ -NMR spectra comparison between maize starch and modified starches. No additional peaks are found in the ES-2 and ES-3 spectra.

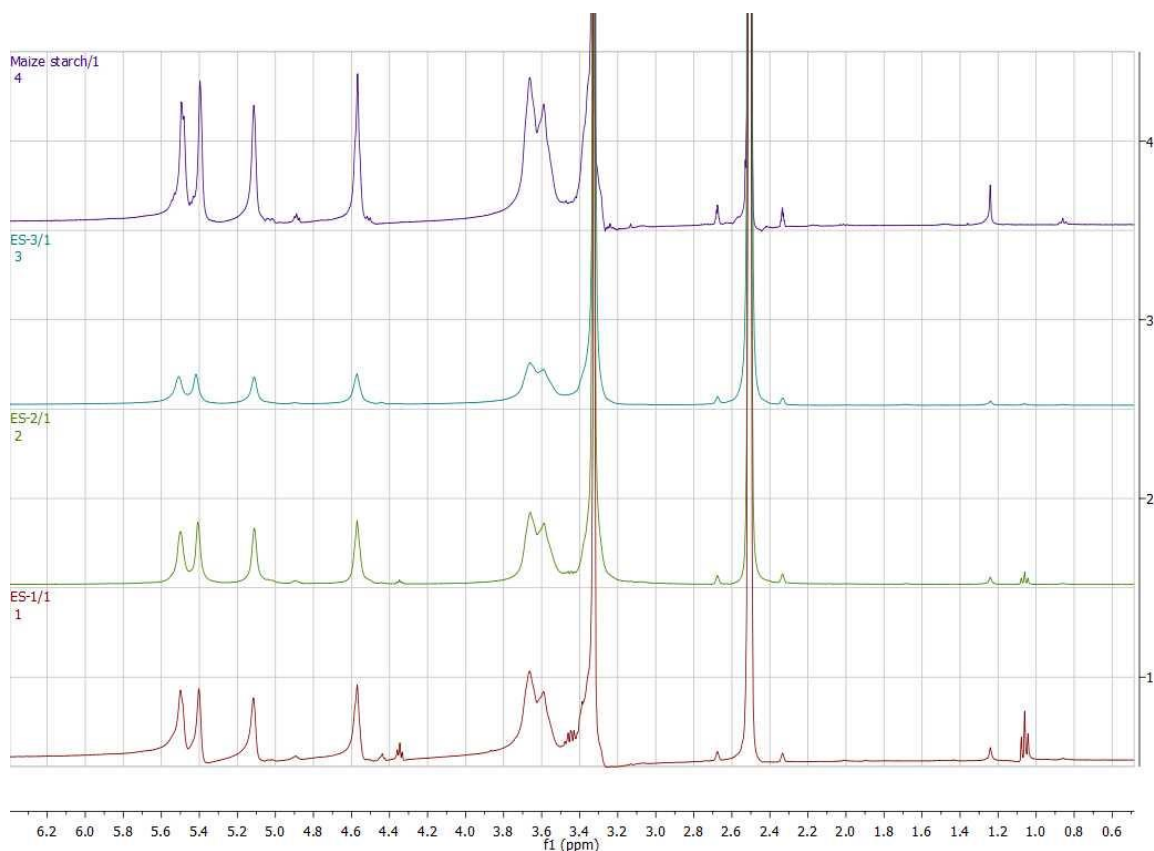


**Figure 5.7:**  $^1\text{H}$ -NMR spectrum of maize starch.

The reaction introduced new peaks in ES-1 as shown in Figure 5.8. The peak at 3.45 ppm can be attributed at the epoxy ring (H-8,9), but the band of the epoxy ring is wide and could be partially covered by the absorption of the  $\text{H}_2\text{O}$  [36]. The peak at 4.35 ppm can be attributed to aliphatic protons of the ether groups (H-8, H-9) [36]. However, probably these new peaks are due to the presence of ethanol impurities, since FTIR analysis doesn't confirm the presence of epoxy rings.

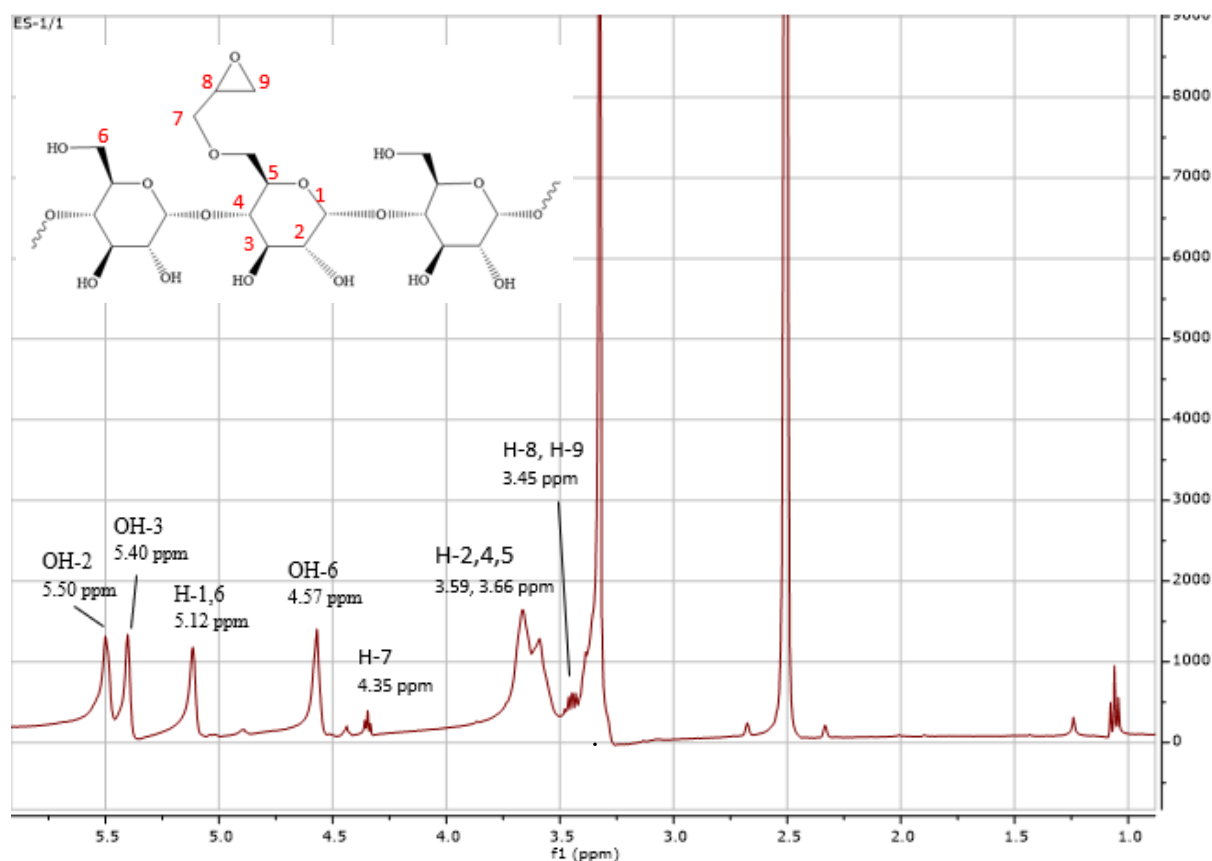


Figure 5.8:  $^1\text{H}$ -NMR spectrum of ES-1 reaction.

### 5.2.2 ES-4, ES-5, ES-6 analysis.

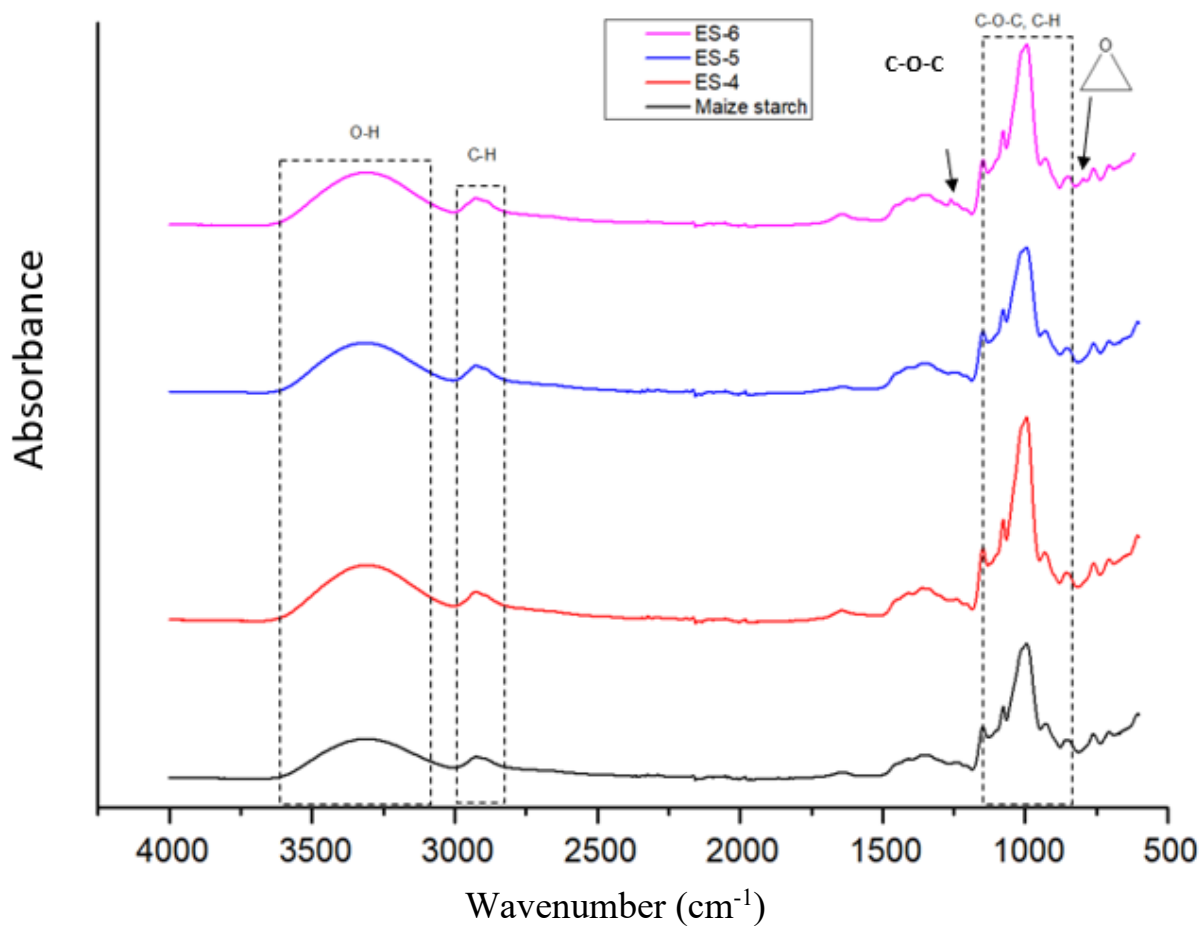
In the following Table 5.4 are shown the reaction conditions of the reactions number 4, 5 and 6.

Table 5.4: Experimental parameters for ES-4, ES-5 and ES-6

Reaction	Starch [g]	ECH [ml]	Molar ratio (ECH: $^1\text{AGU}$ :NaOH)	NaOH Solution [ml]	Time [h]	Temperature [ $^{\circ}\text{C}$ ]
ES-4	1.03	2.49	5:1:-	undefined	2	85
ES-5	1.07	0.52	1:1:-	undefined	2	100
ES-6	1.04	3.52	7:1:1	12.83	5	85

In the FTIR spectra of ES-4 and ES-5 presented in Figure 5.9, where the temperature is increased, no significant change can be noted with respect to the maize starch one. In ES-6 spectrum instead, new peaks at  $1260\text{ cm}^{-1}$  and at  $796\text{ cm}^{-1}$  appeared which are not visible in the native maize starch. The small peak at  $1260\text{ cm}^{-1}$  can be attributed to the stretching vibrations of C-O-C ether bond, (possibly due to a certain amount of opened epoxy ring) [37]. The other peak at  $796\text{ cm}^{-1}$  can be attributed to a monosubstituted epoxy ring [34].

From these results it seems that both the addition of NaOH at the beginning of the reaction and an increased amount of ECH can promote the epoxidation reaction.



**Figure 5.9:** FTIR spectra of maize starch and modified starches ES-6, ES-5, ES-4.

In the ES-4 <sup>1</sup>H-NMR spectra there are not new peaks. In the ES-5 spectrum new small peaks are visible at 3.45 and 4.35 ppm but they could be probably due to the presence of ethanol impurities.

The ES-6 sample was slightly soluble in DMSO-d<sub>6</sub> so the H-NMR spectrum recorded was less clear as it can be seen in the Figure 5.10.

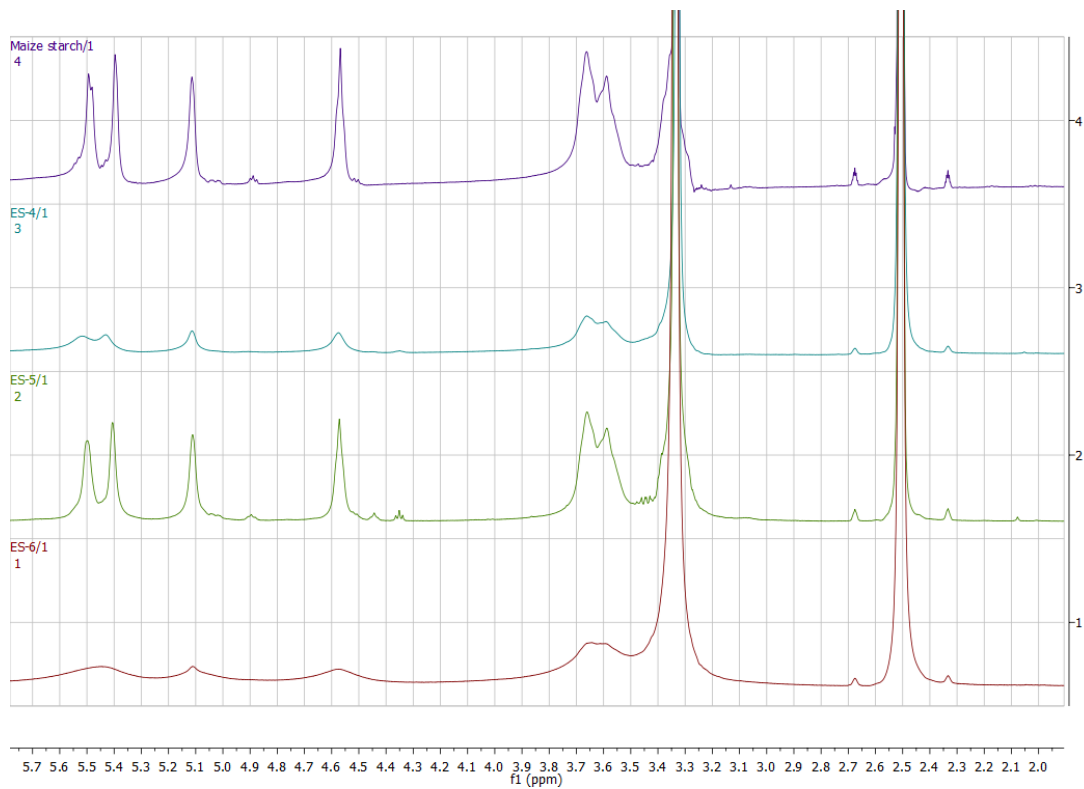


**Figure 5.10:**  $^1\text{H}$ -NMR spectra of maize starch and modified starches ES-4, ES-5, ES-6.

A DSC analysis comparison between native starch, ES-1, ES-3 and ES-6 is shown in the next Figure 5.11.

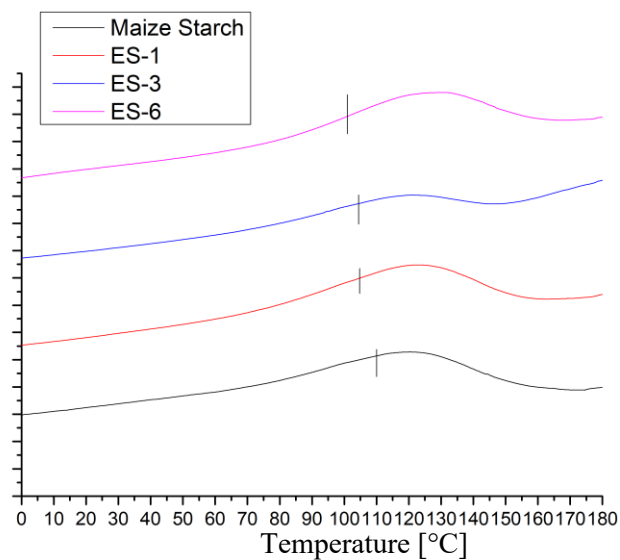


**Figure 5.11:** DSC comparison between Maize starch, ES-1, ES-3 and ES-6

The following Table 5.5 shows the  $T_g$  average of three samples analysed for each product with the appropriate standard deviation.

**Table 5.5:** T<sub>g</sub> of Maize starch, ES-1, ES-3 and ES-6

<b>Glass Transition Temperature [°C]</b>					
	<b>Sample 1</b>	<b>Sample 3</b>	<b>Sample</b>	<b>Average</b>	<b>STD.DEV</b>
<b>Maize Starch</b>	105	107	110	107	2.9
<b>ES-1</b>	105	107	102	104	2.7
<b>ES-3</b>	101	104	108	104	3.5
<b>ES-6</b>	105	102	97	101	4.2

### 5.2.3 ES-9 analysis

The following Table 5.6 shows the reaction conditions of the reaction number 9.

**Table 5.6:** Experimental parameters for ES-9

<b>Reaction</b>	<b>Starch [g]</b>	<b>ECH [ml]</b>	<b>Molar ratio (ECH:AGU:NaOH)</b>	<b>NaOH Solution [ml]</b>	<b>Time [h]</b>	<b>Temperature [°C]</b>
<b>ES-9</b>	1.16	6.70	12:1:12	<b>171.85</b>	5	85

The main difference in this reaction procedure was the addition of a fixed amount of 0.5 M NaOH solution with the starch at the beginning of the experiment, with a molar ratio between NaOH and AGU equal to 12:1. No more addition of the basic solution was necessary during this reaction.

Differently from the previous experiments, the strong basic media allows the complete starch solubilization (not just a starch-water dispersion). Another difference can be seen in the dried product since in this case the particles size is bigger than the one obtained before.

In the ES-9 FTIR spectrum (Figure 5.12) there can be seen two new peaks: one at  $1550\text{ cm}^{-1}$  that can be attributed to the CH<sub>2</sub> of the epoxy ring, the other at  $857\text{ cm}^{-1}$  can be attribute to the vibration of the epoxy ring. Moreover, the bending CH<sub>2</sub> vibration area changes its shape after the reaction. All these results can be explained with a successful attachment of the ECH to the AGU unit without the opening of the epoxy ring.

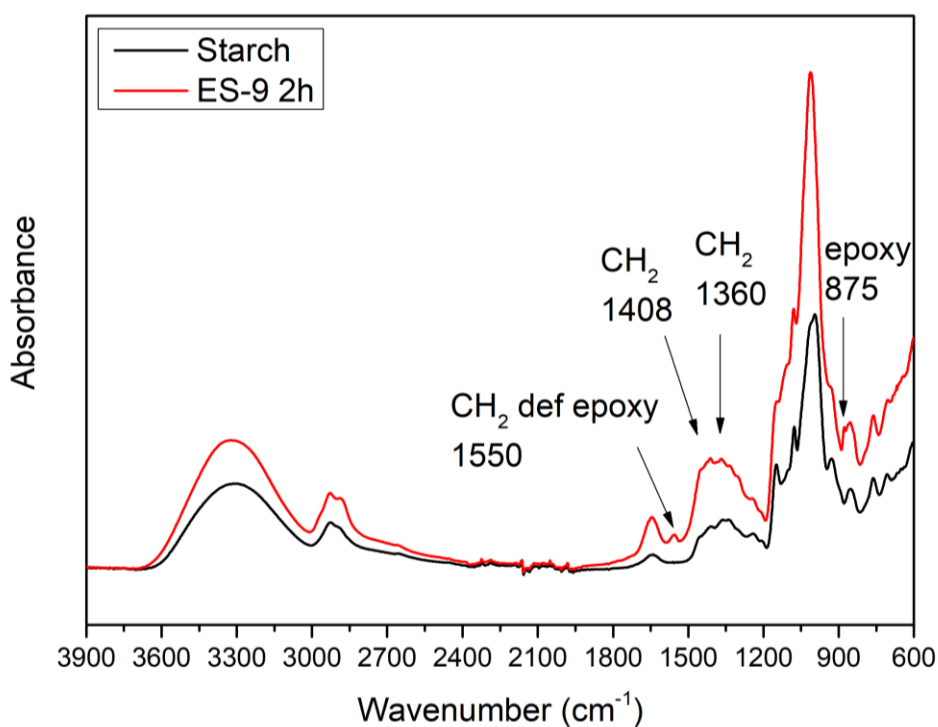


**Figure 5.12:** FTIR spectrum comparison between Maize and ES-9 (2h) starches.

In the  $^1\text{H-NMR}$  spectrum of ES-9 presented in Figure 5.13 some peaks appear confused because the sample wasn't soluble in  $\text{DMSO-d}_6$  and moreover large traces of ethanol remained despite it was dried in a vacuum oven overnight. There is a new peak at 4.35 ppm which can be assigned to the protons of the ether groups. The peak at 3.61 ppm seems wider with respect to the maize starch one, this could be due to the vibration of the protons of the epoxy ring (their peaks can be found in this region of the spectrum). The triplets peak at 3.45 ppm can be assigned to ethanol traces [38].

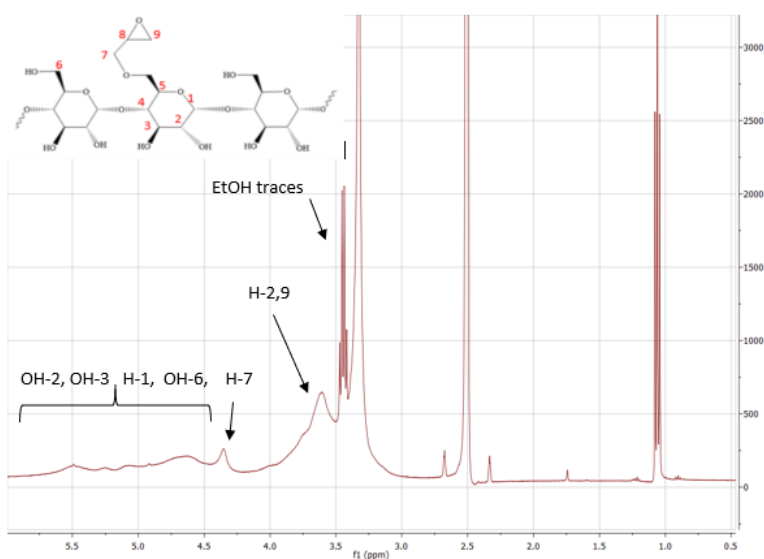


**Figure 5.13:** ES-9  $^1\text{H-NMR}$  spectrum

## 5.2.4 ES-10 analysis

The following Table 5.7 shows the reaction conditions of the reaction number 10.

**Tab 5.7:** Experimental parameters for ES-10

Reaction	Starch	ECH	Molar ratio	NaOH	Time	Temperature
n	h	[ml]	(ECH:AGU*:NaOH)	Solution	[h]	[°C]
	[g]			[ml]		
ES-10	1.06	7,79	15:1:15	196 ml	5h	85

The figure 5.14 shows the FTIR spectra of pristine and the modified ES-10 starch. The ES-10 reported curves were taken from the reaction at different time intervals. An intensity decrease is observed in the OH vibration region, 3650-3000  $\text{cm}^{-1}$  [39] [40] [41] [42] which could be attributed to the proton's substitution in the hydroxyl groups. The peaks at 2921 and 2880  $\text{cm}^{-1}$  are attributed to C-H stretching vibration in  $-\text{CH}_2$  groups [39] [41] [43] [44] [45]. The single peak at 1658  $\text{cm}^{-1}$  is attributed to the water absorbed by starch due its hygroscopic nature [40] [43]. The new single peak at about 1550  $\text{cm}^{-1}$  and the increased intensity of the peak at 1431  $\text{cm}^{-1}$  are attributed to  $-\text{CH}_2-$  bending vibration [34] [39] [40] [45] [46] that could indicate the presence of ether groups. The range between 1366 and 1200  $\text{cm}^{-1}$  is associated to O-H bending of primary or secondary alcohols already present in the native maize starch [40] [47]. The typical peak at 879  $\text{cm}^{-1}$ , which increases its intensity as the reaction proceed, can be assigned to the C-O-C stretching of epoxy ring as confirmed in literature [39] [40] [41] [42] [44] [46] [45] [47]. This band is partially overlapped by C-OH stretching and bending vibrations and by the C-O-C glycosidic bond vibrations [34] [40].

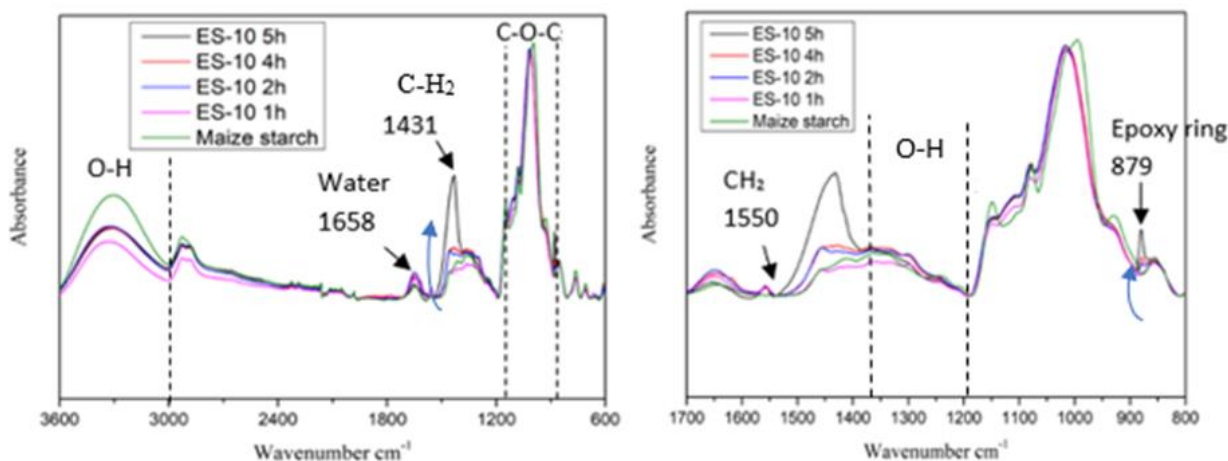


**Fig. 5.14:** FTIR spectra of Maize starch and ES-10.

TGA analysis in the following figure 5.15 show the differences on the thermal stability between the maize starch and the product of ES-10 reaction after 5h. The percentage of volatile component in ES-10 (5h) is 7.8% by weight. The starch degradation starts at around 220 °C. The temperature of the maximum weight loss rate  $T_0 = dm/dT_{max}$  is 260.6 °C. The residual mass  $M_{res}$  at 700°C is 32.2%. This analysis indicates that the product of the reaction is more resistant to heating compared with native starch.

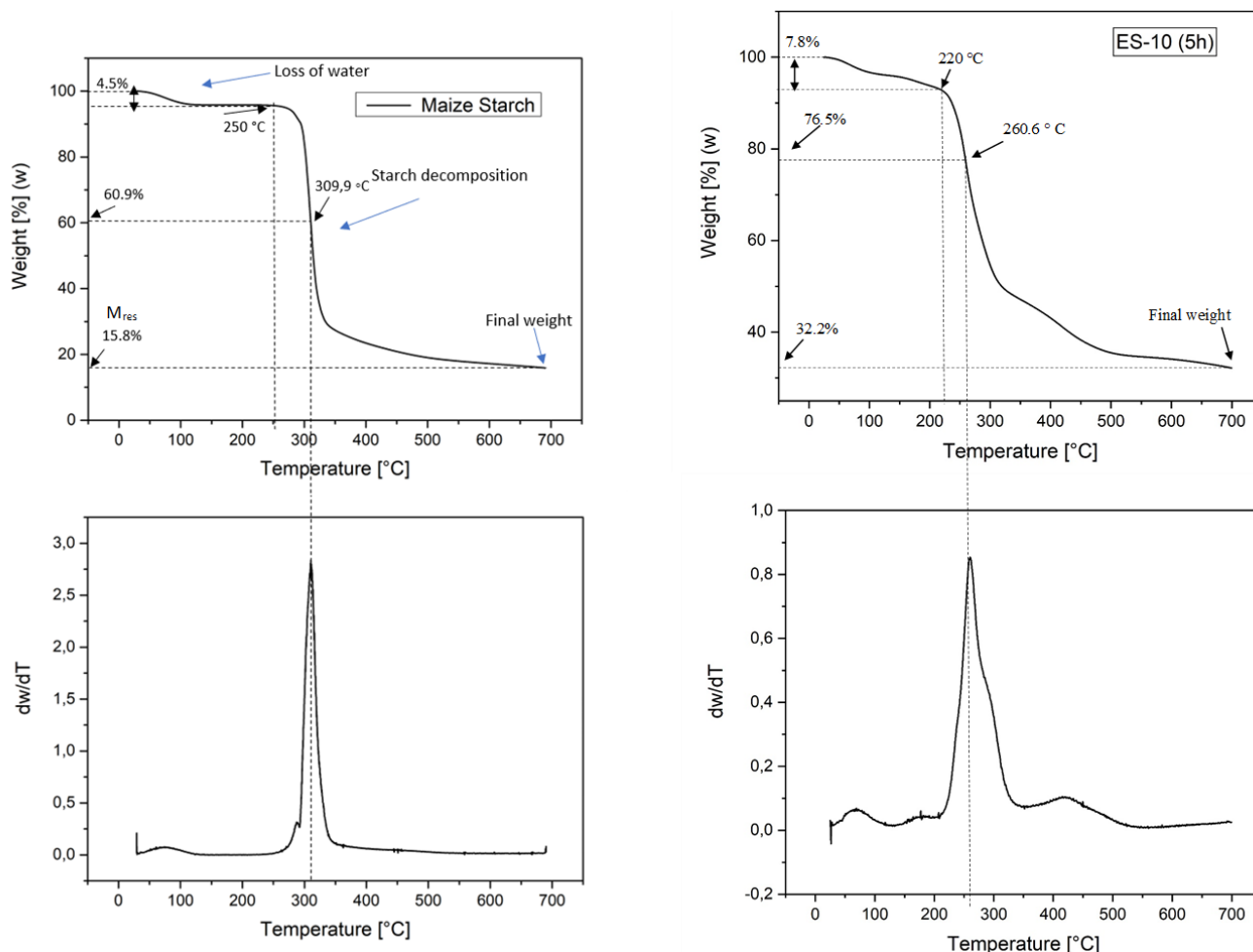


**Figure 5.15:** TGA comparison between maize starch and ES-10 reaction after 5 hours.

However, regioselectivity problems of functionalization could lead to different side reactions, summarized in the next figures 5.16, 5.17 and 5.18.

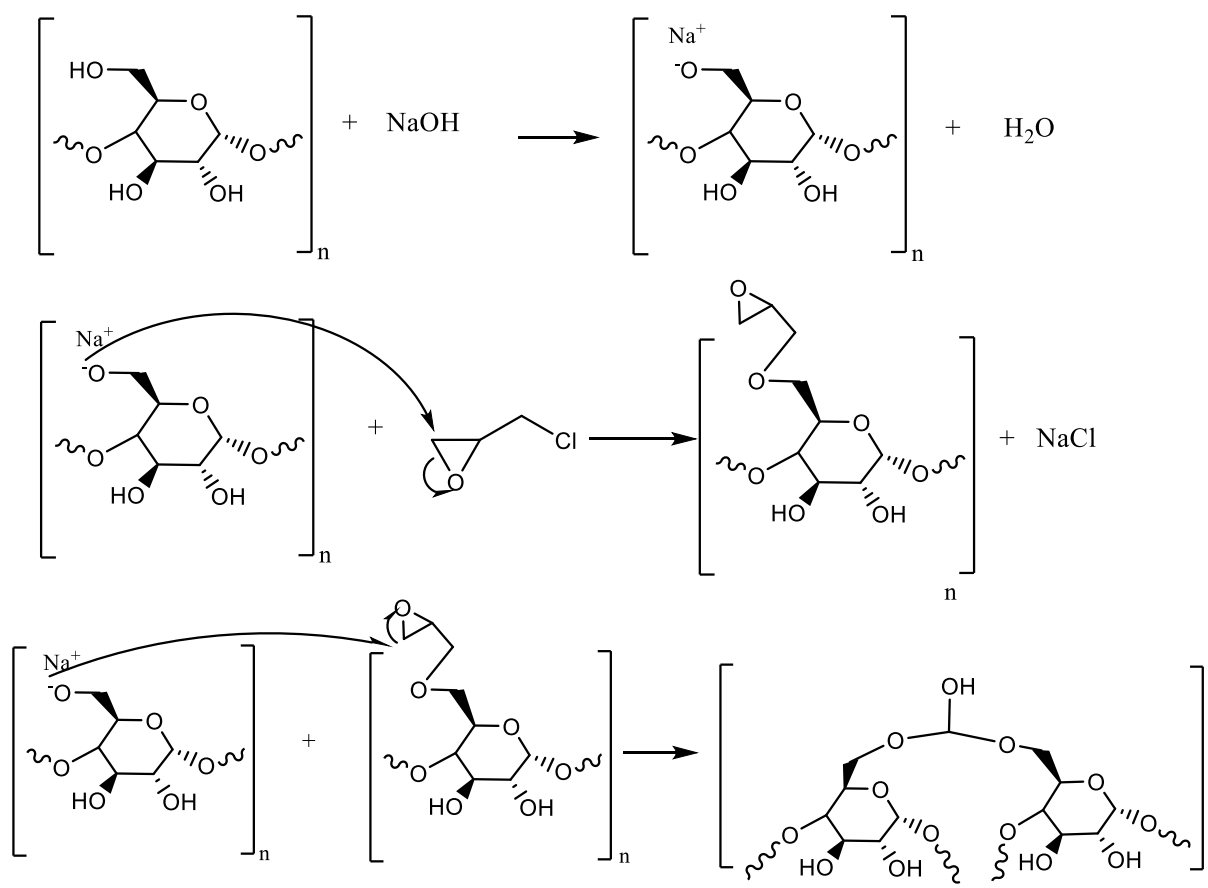


**Fig. 5.16:** Side-reaction 1.

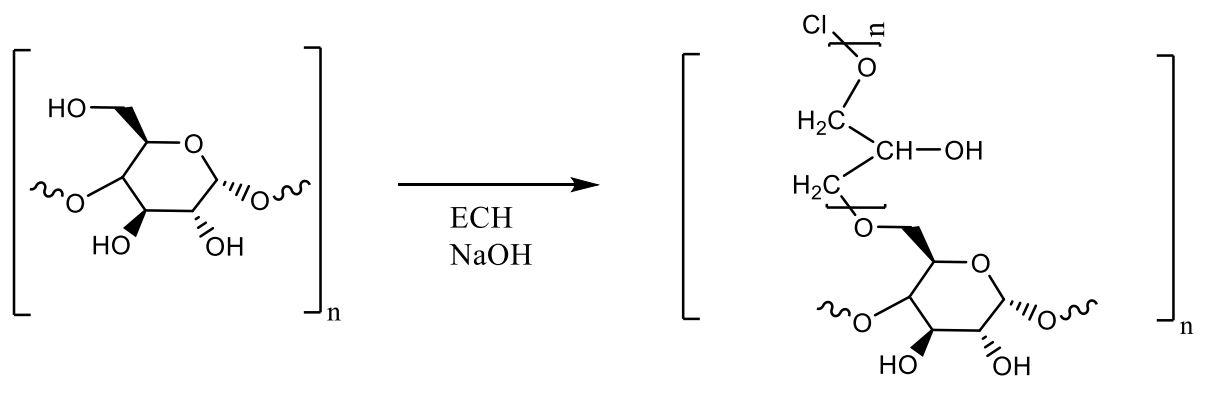


**Fig 5.17:** Side-reaction 2

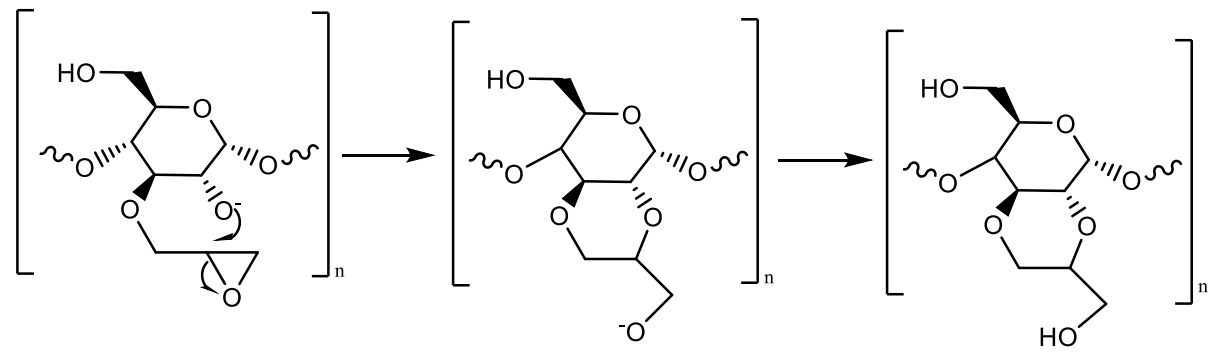


**Fig 5.18:** Side-reaction 3

### 5.2.5 ES-11 analysis

The following Table 5.8 shows the reaction conditions of the reaction number 11.

**Table 5.8:** Experimental parameters for ES-11

Reaction	Starch [g]	ECH [ml]	Molar ratio (ECH:AGU:NaOH)	NaOH Solution [ml]	Time [h]	Temperature [°C]
ES-11	1.05	8,64	17:1:17	220 ml	5h	85

The same result was obtained in the ES-11 reaction (Figure 5.19). A peaks intensity increase is visible at  $879\text{ cm}^{-1}$  (epoxy ring vibration),  $1427$  and  $1550\text{ cm}^{-1}$  ( $\text{CH}_2$ - bending vibrations).

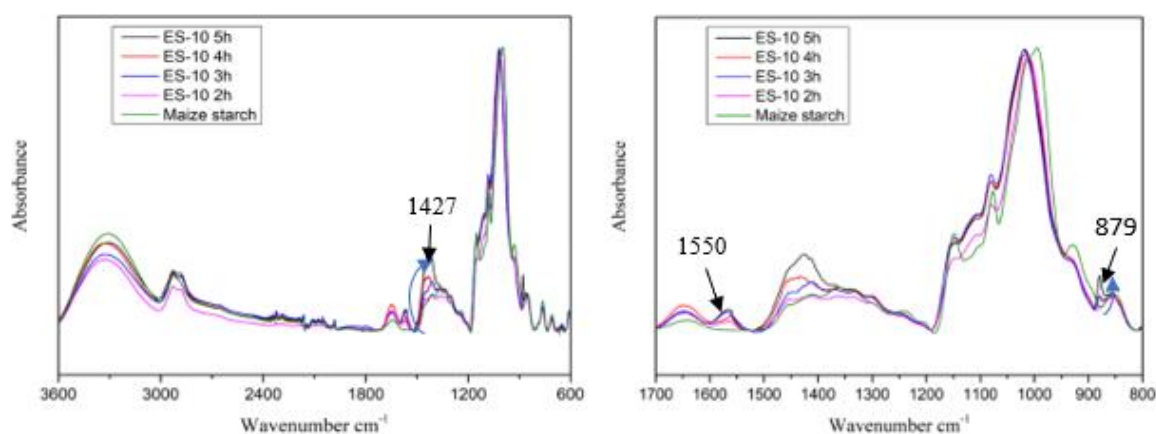


**Fig. 5.19:** FTIR spectra of Maize starch and ES-11.

### 5.2.6 ES-12 analysis

The following Table 5.9 shows the reaction conditions of the reaction number 12.

**Tab 5.9:** Experimental parameters for ES-12

Reaction	Starch [g]	ECH [ml]	Molar ratio (ECH:AGU:NaOH)	NaOH Solution [ml]	Time [h]	Temperature [°C]
ES-12	1.02	9,87	20:1:20	251,8	6h	85

New peaks were observed after 5 and 6 hours (Figure 5.20). The band at  $800\text{ cm}^{-1}$  can be assigned to the characteristic absorption of epoxy ring (symmetric ring deformation) [39] [42] [43] [45] [48]. The  $1260\text{ cm}^{-1}$  peak, previously attribute to the O-H bending of primary and secondary alcohols [40] [47], shows a marked enhancement. This can be explained by the presence of the monosubstituted epoxy ring vibration [34] [42] [49].

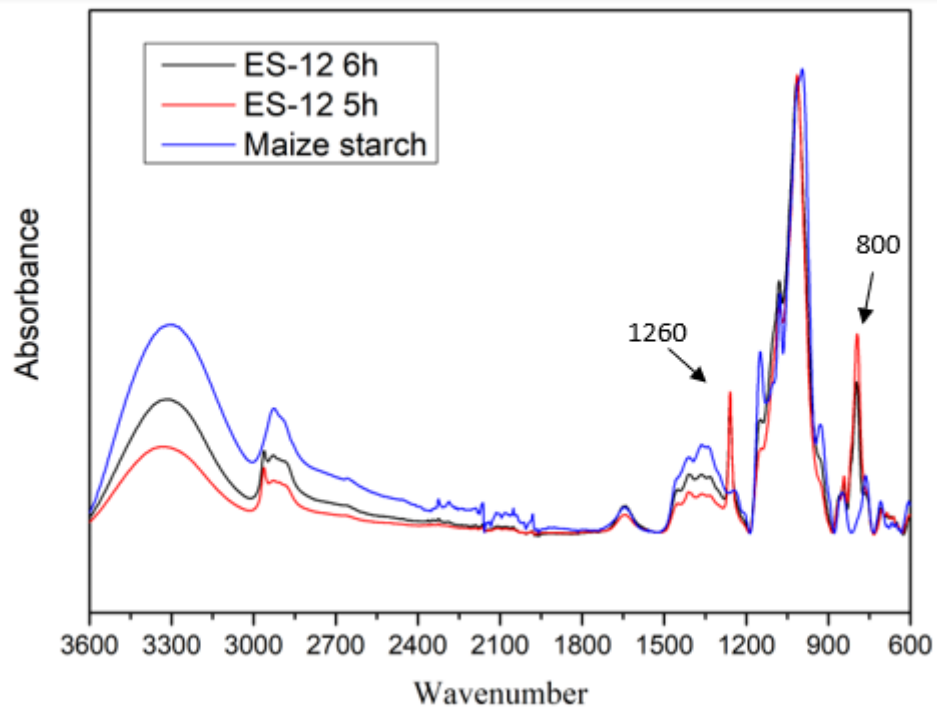


**Figure 5.20:** FTIR spectra of maize starch and ES-12 (5,6 hours).

### 5.3 Methacrylation reaction

The comparison between the  $^1\text{H-NMR}$  spectra of MA-starch and native starch showed in Figure 5.21, confirmed the presence of characteristic peaks assigned to methacrylic double bonds  $=\text{CH}_2$  (5.66 and 6.07 ppm) and to methyl groups  $-\text{CH}_3$  (1.9 ppm). The degree of substitution (DS) can be calculated as the ratio of integrals  $^1\text{H-NMR}$  peaks using the following equation:

$$DS = \left(\frac{I_{4.9}}{I_{5.11}}\right)/3$$

Where:

- $I_{1.9}$  integral intensity of  $\text{CH}_3$  (named b in the spectra)
- $I_{5.11}$  integral intensity of the AGU proton in 1H position ( $\alpha$ -carbon).

The division of the formula by 3 is due to the presence of three  $-\text{OH}$  groups in each AGU. The DS obtained was 0.08 since  $I_{1.9} = 0.75$  and  $I_{5.11} = 1$ . It means that there is only one methacrylated alcohol-group every fourth AGU (Fig. 5.20) [50].

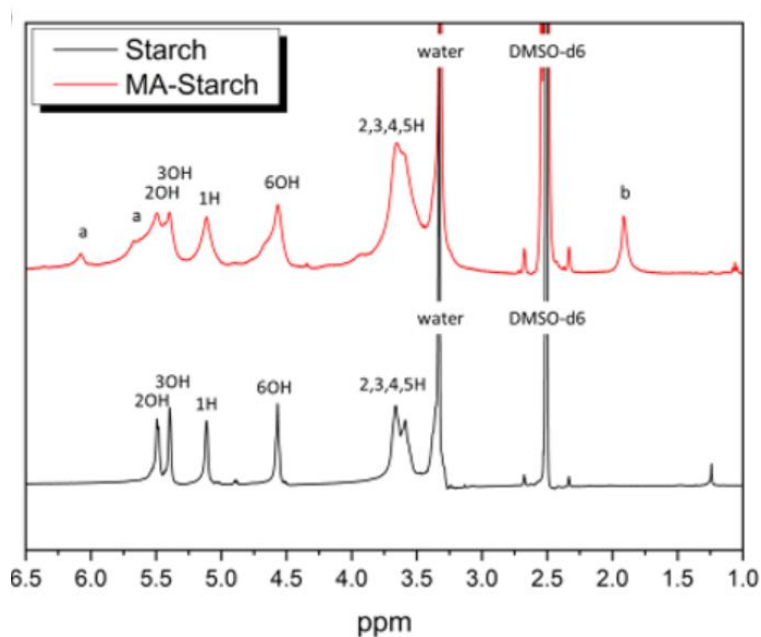


**Figure 5.21:**  $^1\text{H-NMR}$  spectra for native starch and methacrylated MA-starch [50].

In figure 5.22 are shown the  $^{13}\text{C-NMR}$  spectra of MA-Starch and Starch-reference. It can be clearly seen the signals of the methacrylated group at 18.45 ppm (methyl carbon), 136.61 and 127.75 ppm (double bond carbons) and the 170.38 ppm attributed to the  $\text{C}=\text{O}$  carbon [50].

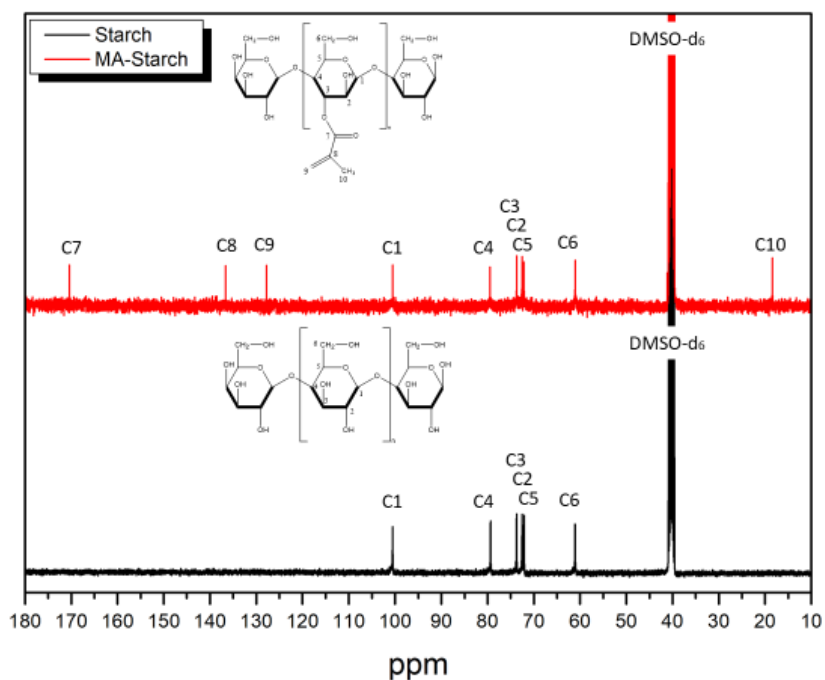


**Figure 5.22:**  $^{13}\text{C}$ -NMR spectra for native starch and MA-starch [50].

The Figure 5.23 reports the FTIR spectra comparison between starch and MA-starch. In the FTIR spectrum of MA-Starch there can be seen two new sharp peaks at  $1709$  and  $1640\text{ cm}^{-1}$  that can be attributed to the  $\text{C}=\text{O}$  and  $-\text{CO}-$  esters stretching vibrations respectively as well as two new peaks at  $1300$  and  $815\text{ cm}^{-1}$  that can be attributed to  $\text{C}=\text{C}-\text{H}$  and  $\text{C}=\text{C}$  vibrations respectively. These results suggest a successful graft of methacrylate groups on the structure of starch [50].

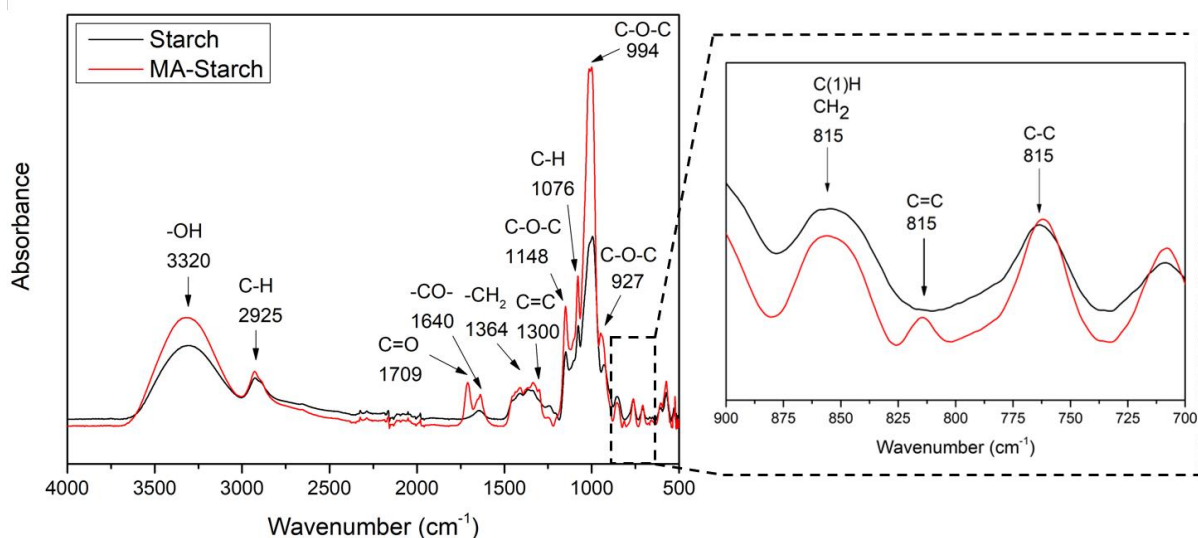


**Figure 5.23:** FTIR spectra of native starch and MA-starch [50].

## 6. Conclusions and future works

In this study, the synthesis of epoxidized and methacrylated starch were performed. The reaction products were tested with spectroscopic and thermal analysis.

Epoxidation reactions produced relevant results from the 9<sup>th</sup> reaction, when a fixed amount of 0.5 M NaOH solution was used at the beginning of the experiment instead of distilled water. The presence of -CH<sub>2</sub>- and of epoxy ring C-O-C was confirmed through the ATR-FTIR analysis. In particular, by monitoring the 10<sup>th</sup> at different time intervals, a progressive increase of these peaks was detected.

The methacrylation reaction produced interesting and significant results. The presence of methacrylic double bonds =CH<sub>2</sub> and methyl groups -CH<sub>3</sub> was confirmed through the spectroscopic analysis and the calculation of the degree of substitution.

The main problems were related to <sup>1</sup>H-NMR analysis, because the epoxidized starch derivatives were not soluble in DMSO-d<sub>6</sub>, making the spectra difficult to analyse. In future works, <sup>1</sup>H-NMR could be performed at high temperature to solve this problem.

In order to calculate the degree of substitution of epoxy rings replacing the -OH groups of the glucose unit, titration techniques could be carried out. However, it is not easy finding a suitable solvent able to dissolve the reaction products properly.

The promising results obtained after both the epoxidation and methacrylation reactions provide framework for future studies to assess their processability with photo-curing techniques.



## References

- [1] Telmo Ojeda, *Polymers and the Environment*. [Online] Available: <https://www.intechopen.com/books/polymer-science/polymers-and-the-environment> [Visited on 22-05-2020].
- [2] Abhilash, M., & Thomas, D. “Biopolymers for Biocomposites and Chemical Sensor Applications”. *Biopolymer Composites in Electronics*. Elsevier Inc. 2017.
- [3] Ibrahim M. S, Hamza M. Y., M. Fazal-ur-Rehman, Zaharadeen I. M, Sirajo I. “Biopolymer Materials, an Alternative to Synthetic Polymer Materials”. *International Invention of Scientific Journal*, Vol. 02(08), pp. 286-295, 2018.
- [4] [Online] Available: <https://www.ciclia.it/item/compostabile-e-biodegradabile.html> [visited on 23-05-2020].
- [5] [Online] Available: <https://www.bioplasticsmagazine.com/en/news/meldungen/20200127-The-global-bio-based-polymer-market-in-2019-A-revised-view.php> [Visited on 18-06-2020]
- [6] Błędzki A. K., Jaszkiwicz A., Urbaniak M., & Stankowska-Walczak D. “Biocomposites in the past and in the future”. *Fibres and Textiles in Eastern Europe*, Vol. 96(6B), pp. 15–22, 2012.
- [7] [Online] Available: <http://www.disegnoindustriale.net/diid/bioplastics-dai-polimeri-ai-biopolimeri/> [visited on 21-04-2020].
- [8] Biswajit Maji. “Introduction to natural polysaccharides”. *Functional Polysaccharides for Biomedical Applications*. [Online] Available: <https://doi.org/10.1016/B978-0-08-102555-0.00001-7>.
- [9] [Online] Available: <http://www.nutrientsreview.com/carbs/monosaccharides-simple-sugars.html> [visited on 22-04-2020].
- [10] Cumpstey I. “Review Article: Chemical Modification of Polysaccharides”. *ISRN Organic Chemistry*. Vol. 2013., pp. 383–406, 2013.
- [11] Chen Q., Yu H., Wang L., Ul Abdin Z., Chen Y., Wang J., Zhou W., Yang X., Khan R. U., Zhang H., & Chen X. “Recent progress in chemical modification of starch and its applications”. *RSC Advances*, Vol. 5(83), pp. 67459–67474, 2015.
- [12] M.G. Sajilata, Rekha S. Singhal, and Pushpa R. Kulkarni. “Resistant Starch – A Review”. *Comprehensive Reviews In Food Science And Food Safety*. Vol. 5, 2006.
- [13] Mei-Yu Chen, Guan-Yu Zhuo, Kuan-Chieh Chen, Pei-Chun Wu, Tsung-Yuan Hsieh, Tzu-Ming Liu & Shi-Wei Chu. “Multiphoton imaging to identify grana, stroma thylakoid, and starch inside an intact leaf”. *BMC Plant Biology*, Vol. 14(175), 2015.
- [14] Pontis H. G. (2017). “Case Study: Starch”. *Book: Methods for Analysis of Carbohydrate Metabolism in Photosynthetic Organisms*, Chapter 11, pp. 151–167, 2017.

- [15] Ratnayake W. S. & Jackson D. S. “Chapter 5: Starch Gelatinization”. *Advances in Food and Nutrition Research*, Vol. 55(08), pp. 221–268, 2008.
- [16] [Online] Available: <https://www.allaboutfeed.net/Equipment/Articles/2018/2/Gelatinised-extruded-feed-Does-it-matter-253018E/> [Visited on 24-04-2020].
- [17] Masina N., Choonara Y. E., Kumar P., du Toit L. C., Govender M., Indermun S., & Pillay V. “A review of the chemical modification techniques of starch”. *Carbohydrate Polymers*, Vol. 157, pp. 1226–1236, 2017
- [18] Beckles D. M. & Maysaya T. (2016). “Use of Biotechnology to Engineer Starch in Cereals” *Encyclopedia of Biotechnology in Agriculture and Food*, pp. 1–8. 2014
- [19] Silva D. A., De Paula R. C. M., Feitosa J. P. A., De Brito A. C. F., Maciel J. S., & Paula H. C. B. “Carboxymethylation of cashew tree exudate polysaccharide”. *Carbohydrate Polymers*, Vol. 58(2), pp. 163–171, 2004.
- [20] Henry O. E. “Chapter: Chemical Properties of Starch and Its Application in the Food Industry”. [Online] Available: <http://dx.doi.org/10.5772/intechopen.87777>. [Visited on 29-04-2020]
- [21] Huijbrechts A. M. L., Haar, R. ter, Schols H. A., Franssen M. C. R., Boeriu C. G., & Sudhölter E. J. R. “Synthesis and application of epoxy starch derivatives”. *Carbohydrate Polymers*, Vol. 79(4), pp. 858–866, 2010.
- [22] Pagliaro M. “Chapter 2: C3-Monomers”. *Glycerol*. 2017. [Online] Available: <http://dx.doi.org/10.1016/B978-0-12-812205-1.00002-3>. [Visited on 29-04-2020].
- [23] [Online] Available: [http://www.chemgapedia.de/vsengine/vlu/vsc/en/ch/2/vlu/oxidation\\_reduktion/and\\_epoxi.vlu/Page/vsc/en/ch/2/oc/reaktionen/formale\\_systematik/oxidation\\_reduktion/oxidation/addition\\_sauerstoff/andere\\_epoxidierungsverfahren/chlorhydrin.vscml.html](http://www.chemgapedia.de/vsengine/vlu/vsc/en/ch/2/vlu/oxidation_reduktion/and_epoxi.vlu/Page/vsc/en/ch/2/oc/reaktionen/formale_systematik/oxidation_reduktion/oxidation/addition_sauerstoff/andere_epoxidierungsverfahren/chlorhydrin.vscml.html) [Visited on 29-04-2020].
- [24] Hamdi G., Ponchel G., & Duchêne D. “Formulation of epichlorohydrin cross-linked starch microspheres”. *Journal of Microencapsulation*, Vol. 18(3), pp. 373–383, 2001.
- [25] Hedin J., Östlund Å., & Nydén M. “UV induced cross-linking of starch modified with glycidyl methacrylate”. *Carbohydrate Polymers*, Vol. 79(3), pp. 606–613, 2010.
- [26] Wöhl-Bruhn S., Bertz A., Harling S. H., & Bunjes H. “Hydroxyethyl starch-based polymers for the controlled release of biomacromolecules from hydrogel microspheres”. *European Journal of Pharmaceutics and Biopharmaceutics*, Vol. 81(3), pp. 573–581, 2012.
- [27] [Online] Available: <https://www2.chemistry.msu.edu/faculty/reusch/VirtTxtJml/Spectrpy/nmr/nmr1.htm> [Visited on 07-06-2020].
- [28] [Online] Available: [http://www.unimegroup.it/uploads/files/chimica-e-tecnologia-farmaceutiche/spettroscopia-nmr/lo\\_spetro\\_13c\\_nmr.pdf](http://www.unimegroup.it/uploads/files/chimica-e-tecnologia-farmaceutiche/spettroscopia-nmr/lo_spetro_13c_nmr.pdf). [Visited on 15-06-2020].

- [29] [Online] Available: <https://lotusgemology.com/index.php/2-uncategorised/294-ftir-in-gem-testing-ftir-intrigue-lotus-gemology> [Visited on 16-06-2020]
- [30] [Online] Available: <https://www.netzsch-thermal-analysis.com/en/landing-pages/principle-of-a-heat-flux-dsc/> [Visited on 16-06-2020].
- [31] [Online] Available: International Thermoplastics Testing Center UL <https://www.ulttc.com/it/soluzioni/metodi-di-prova/analisi-termica/analisi-termogravimetricatga.html> / (Online Resource visited on 16-06-2020)
- [32] Christine Geers. Inhibition of coking and metal dusting on conventional alloys by using a nickel-tin intermetallic coating. *PhD Thesis*, Jan. 2013.
- [33] Ramazan Kizil, Joseph Irudayaraj, Koushik Seetharaman. Characterization of Irradiated Starches by Using FT-Raman and FTIR Spectroscopy. *J. Agric. Food Chem.* 2002, 50, 3912-3918.
- [34] Socrates George, Infrared and Raman Characteristic Group Frequencies, New York, John Wiley & Sons, LTD, 2001.
- [35] Duo Wu and Minna Hakkarainen. A Closed-Loop Process from Microwave-Assisted Hydrothermal Degradation of Starch to Utilization of the Obtained Degradation Products as Starch Plasticizers. *ACS Sustainable Chem. Eng.* 2014, 2, 2172–2181.
- [36] Deepak M. Patil, Ganesh A. Phalak, S. T. Mhaske. Synthesis of bio-based epoxy resin from gallic acid with various epoxy equivalent weights and its effects on coating properties. *J. Coat. Technol. Res.*, 2017, 14 (2), 355–365.
- [37] I. Rute Fontinha, M. Manuela Salta, Mikhail L. Zheludkevich and Mário G.S. Ferreira. EIS Study of Amine Cured Epoxy-silica-zirconia Sol-gel Coatings for Corrosion Protection of the Aluminium Alloy EN AW 6063. *Portugaliae Electrochimica Acta* 2013, 31(6), 307-319.
- [38] Ioannis P. Gerothanassis, Anastassios Troganis, Vassiliki Exarchou and Klimentini Barbarossou. Nuclear Magnetic Resonance (NMR) spectroscopy: basic principles and phenomena, and their applications to chemistry, biology and medicine. *Chemistry education: research and practice in Europe.* 2002, Vol. 3, No. 2, 229-252
- [39] Panamgama LA, Peramune PRUSK. Extraction and modification of lignin biopolymer. *3rd Int Moratuwa Eng Res Conf MERCon.* 2017. 13-16.
- [40] Pozo C, Rodríguez-Llamazares S, Bouza R, et al. Study of the structural order of native starch granules using combined FTIR and XRD analysis. *J Polym Res.* 2018. 25(12).
- [41] M Sain NY. A New Method for Demethylation of Lignin from Woody Biomass using Biophysical Methods. *J Chem Eng Process Technol.* 2013. 04(09).
- [42] Kiran V, Gaur B. Curing and thermal behavior of epoxy resins of hexafluoro-bisphenol-A and bisphenol-A. *Polimeros.* 2016. 26(1), 11-20.

- [43] Taghavian H, Ranaei-Siadat S-O, Kalae MR, Mazinani S. Investigation of the effects of starch on the physical and biological properties of polyacrylamide (PAAm)/starch nanofibers. *Prog Biomater*. 2017. 6(3), 85-96.
- [44] Lu S, Ban J, Yu C, Deng W. Properties of epoxy Resins modified with liquid crystalline polyurethane. *Iran Polym J (English Ed)*. 2010. 19(9), 669-678.
- [45] Liu J, Tang J, Wang X, Wu D. Synthesis, characterization and curing properties of a novel cycloliner phosphazene-based epoxy resin for halogen-free flame retardancy and high performance. *RSC Adv*. 2012. 2(13), 5789-5799.
- [46] Cakić SM, Ristić IS, Jašo VM, Radičević RŽ, Ilić OZ, Simendić JKB. Investigation of the curing kinetics of alkyd-melamine-epoxy resin system. *Prog Org Coatings*. 2012. 73(4), 415-424.
- [47] John Coates. Interpretation of Infrared Spectra, A Practical Approach. *Encyclopedia of Analytical Chemistry*. 2000. 10815-10837
- [48] Wang Y, Li H, Wang X, Lei H, Huo J. Chemical modification of starch with epoxy resin to enhance the interfacial adhesion of epoxy-based glass fiber composites. *RSC Adv*. 2016;6(87):84187-84193.
- [49] Jahanshahi S, Pizzi A, Abdulkhani A, Shakeri A. Analysis and testing of bisphenol a-free bio-based tannin epoxy-acrylic adhesives. *Polymers (Basel)*. 2016. 8(4).
- [50] Camilla Noè, Chiara Tonda-Turo, Annalisa Chiappone, Marco Sangermano and Minna Hakkarainen. Light Processable Starch Hydrogels. *Polymers*. 2020. 12, 1359.



## Acknowledgments

First, I would like to thank my Relators Marco Sangermano and Minna Hakkarainen for their special advices and the great opportunity to carry out this project in Stockholm. This allowed me to work in a great environment, to meet beautiful people and to create my future.

I would like to extend my sincere gratitude to my Tutor Camilla for its patience. I wish to everyone to have a guide like her. Her advices and corrections will be important in my future work.

I would like to thank all the Department of Fibre and Polymer Technology of KTH for helping during my project, especially to my officemate Karin for her support.

I would like to really thank my parents Salvatore and Liliana who have always encouraged me to not give up despite adversity and have supported me economically in my university years. Without them all this would not have been possible. I feel immense admiration for you and your love will be always an example for my future.

I would like to thank my brother Giampiero and his wife Lidia for putting me in a good mood and sending me always positivity messages. They represented a source of inspiration for me. Thank you for giving us Edoardo, our family jewel.

A special thanks to my girlfriend, Martina. A brilliant, solar and unique person. We shared joys and sorrows, ups and downs and then ended this journey together. You are a friend, a partner and a reference point.

I would like to thank my friend Giacc for his availability and for his kindness. I wish you well, always.

A special thanks to Davide, Benny and Antonella. Even if we are often far away you will be always in my heart.

Lastly, I would like to thank all my special friends of Turin and Sicily.

